People`s Democratic Republic of Algeria
Ministry of Higher Education and Scientific Research
University of Echahid Hamma Lakhdar - El Oued
Faculty of Technology
Department of Mechanical Engineering
Dissertation
ACADEMIC MASTER
Domain: **Science and Technology**
Division: **Mechanical Engineering**
Specialty: **Industrial Maintenance**

Presented by:

1. BEN AISSA IDRIS
2. CHETTI NIDAL
3. DIAB HACEN

Entitled:

Enhanced Fault Detection in Photovoltaic Systems via I-V Curve Analysis and Artificial Intelligence Techniques

Dissertation Submitted in Partial Fulfillment of the Requirements for the Master

MEM

Degree in Industrial Maintenance

Publicly defended in: 23/05 /2026

Board of Examiners:

Dr. Mahmoudi Abdelkader	Chairman
Dr. Ali Bebboukha	Supervisor
Dr.Milodie Khaled	Examiner

Academic Year: 2025/2026

ACKNOWLEDGEMENTS

We would like to express our sincere gratitude to our supervisor for his valuable guidance, continuous support, and helpful advice throughout the preparation of this thesis. We would also like to thank the members of the examination committee for reviewing this work and for their constructive comments and suggestions that contributed to improving its quality. Our sincere thanks also go to the professors of the Faculty of Technology who guided and taught us throughout the past five years, contributing greatly to our academic development. Finally, we would like to express our appreciation to University of Echahid Hamma Lakhdar El Oued for providing the academic environment and resources that enabled us to successfully complete our studies and accomplish this work.

DEDICATION

To my beloved parents, who were the light that guided my path and the support that gave me the strength to continue my journey.

To my dear brothers, who have always been a source of support and encouragement in my life.

To my loyal friends, who shared with me the moments of effort and success.

To those who left this world but remain in our hearts as cherished memories. May God have mercy on them and grant them eternal peace.

And to everyone who supported me and stood by my side in completing this work.

BEN AISSA IDRIS

DEDICATION

To my parents, whose love, support, and care have helped me get to where I am today.

To my brothers, who have been my strength in difficult times.

To my friends, who have shared good times and bad times.

And to all who believed in me and encouraged me along the way, know that you are a part of this achievement.

CHETTI NIDAL

DEDICATION

To my beloved parents,

Thank you for your endless love, support, and prayers. Your unwavering belief in me has been my greatest motivation.

To my respected teacher,

I deeply appreciate your guidance, patience, and the knowledge you have shared. You have been a true inspiration.

To my dear friends,

Thank you for your constant encouragement, laughter, and companionship.

Your presence has made this journey more meaningful. With heartfelt gratitude, I dedicate this work to you all.

DIAB HACEN

Abstract

This work focuses on enhancing fault detection in photovoltaic (PV) systems by combining current–voltage (I–V) curve analysis with artificial intelligence techniques. As the demand for renewable energy continues to grow, PV systems have become a key solution due to their sustainability and environmental benefits. However, their performance is often affected by environmental conditions such as dust, shading, humidity, temperature variations, and system degradation.

In this study, an experimental setup based on a DC/DC buck-boost converter was developed to extract real-time I–V characteristics of PV systems. These characteristics were analyzed under different fault conditions to understand their impact on system performance. Furthermore, artificial intelligence models were applied to classify and diagnose faults accurately by learning patterns from the extracted data.

The results demonstrate that combining I–V curve analysis with AI significantly improves fault detection accuracy and system reliability compared to traditional methods. This approach enables early detection of anomalies, reduces maintenance costs, and enhances the overall efficiency and lifespan of photovoltaic systems. Ultimately, this research contributes to the development of smarter and more sustainable solar energy systems.

Keywords: Photovoltaic Systems , Fault Detection ,I–V Curve Analysis , Artificial Intelligence , Machine Learning , Renewable Energy

Résumé :

Ce travail vise à améliorer la détection des défauts dans les systèmes photovoltaïques (PV) en combinant l'analyse des courbes courant–tension (I–V) avec des techniques d'intelligence artificielle. Avec la croissance de la demande en énergies renouvelables, les systèmes PV représentent une solution durable et respectueuse de l'environnement. Cependant, leurs performances sont souvent affectées par des facteurs environnementaux tels que la poussière, l'ombrage, l'humidité, les variations de température et la dégradation des composants.

Dans cette étude, un dispositif expérimental basé sur un convertisseur DC/DC buck-boost a été développé pour extraire en temps réel les caractéristiques I–V des systèmes PV. Ces caractéristiques ont été analysées sous différentes conditions de défaut afin d'évaluer leur impact sur les performances du système. Par ailleurs, des modèles d'intelligence artificielle ont été utilisés pour classifier et diagnostiquer les défauts avec précision.

Les résultats montrent que la combinaison de l'analyse des courbes I–V et de l'intelligence artificielle améliore considérablement la précision de détection des défauts et la fiabilité du système par rapport aux méthodes classiques. Cette approche permet une détection précoce des anomalies, une réduction des coûts de maintenance et une amélioration de l'efficacité et de la durée de vie des systèmes photovoltaïques. Ce travail contribue ainsi au développement de systèmes solaires plus intelligents et durabl.

Mots-clés : Systèmes photovoltaïques, Détection de défauts, Analyse des courbes I-V, Intelligence artificielle, Apprentissage automatique, Énergies renouvelables

ملخص :

يركّز هذا العمل على تحسين كشف الأعطال في الأنظمة الكهروضوئية (PV) من خلال دمج تحليل منحنيات التيار–الجهد (I–V) مع تقنيات الذكاء الاصطناعي. ومع استمرار تزايد الطلب على الطاقة المتجددة، أصبحت الأنظمة الكهروضوئية حلاً أساسياً بفضل استدامتها وفوائدها البيئية. ومع ذلك، فإن أداء هذه الأنظمة يتأثر غالبًا بالظروف البيئية مثل الغبار، والتظليل، والرطوبة، وتغيرات درجة الحرارة، إضافةً إلى تدهور مكونات النظام مع الزمن.

في هذه الدراسة، تم تطوير منصة تجريبية تعتمد على محول DC/DC من نوع Buck-Boost لاستخراج خصائص التيار–الجهد للأنظمة الكهروضوئية بشكل آني. وقد تم تحليل هذه الخصائص تحت ظروف أعطال مختلفة لفهم تأثيرها على أداء النظام. بالإضافة إلى ذلك، تم تطبيق نماذج الذكاء الاصطناعي لتصنيف وتشخيص الأعطال بدقة من خلال تعلم الأنماط المستخلصة من البيانات.

أظهرت النتائج أن الجمع بين تحليل منحنيات التيار–الجهد وتقنيات الذكاء الاصطناعي يحسن بشكل كبير دقة كشف الأعطال وموثوقية النظام مقارنة بالطرق التقليدية. كما تتيح هذه المقاربة الكشف المبكر عن الحالات غير الطبيعية، وتقليل تكاليف الصيانة، وتحسين الكفاءة العامة والعمر التشغيلي للأنظمة الكهروضوئية. وفي النهاية، يساهم هذا البحث في تطوير أنظمة طاقة شمسية أكثر ذكاءً واستدامة

الكلمات المفتاحية: أنظمة الخلايا الكهروضوئية، كشف الأعطال، تحليل منحنى التيار-الجهد، الذكاء الاصطناعي، التعلم الآلي، الطاقة المتجددة

Contents

Chapter I

Solar Radiation and Photovoltaic Energy

Chapter II

Modeling and control of photovoltaic systems

Chapter III

Test and Application

Chapter IV

AI-Based Fault Diagnosis of Photovoltaic Systems Using I–V Curve Analysis

List of Figures

List of Tables

General Introduction

General Introduction :

Global interest in renewable energy sources has grown because of increased demand for electricity, environmental worries, and the shrinking supply of fossil fuels. Photovoltaic (PV) systems stand out considering their sustainability, ability to be scaled, and low environmental impact. PV systems are now common in different places around the world, both as stand-alone setups and connected to power grids.

Even with their benefits, PV systems are subject to changing conditions like variations in solar power, temperature changes, and gradual wear and tear. These things can cause issues that hurt how well the system works, lower energy output, and shorten its lifespan. Often, these issues develop slowly and aren't found by standard monitoring methods, so better diagnostic tools are needed.

Electrical properties, like current–voltage (I–V) curves, give a clear picture of how PV systems are working. Changes in these curves usually point to problems or unusual conditions. But, reading I–V curves can be hard when the environment is always changing, making basic or manual ways of finding problems not good enough.

Recently, artificial intelligence (AI) has shown it can handle these difficulties by smartly looking at complicated data. When AI is used to keep an eye on PV systems, it can get better at spotting problems by learning what normal and problem states look like. This leads to quicker discovery, better correctness, and improved reliability compared to regular methods.

This paper focuses on improving problem detection in PV systems by using both I–V curve study and AI. By making a smart diagnostic system, this work hopes to make systems more trustworthy, make maintenance better, and help create PV energy systems that are more useful and lasting.

systems.

Chapter I

Solar Radiation and Photovoltaic Energy

I.1. Introduction :

Solar radiation represents the most plentiful energy resource available on Earth and serves as the fundamental energy input for photovoltaic (PV) systems. Photovoltaic energy, commonly known as solar energy, is obtained through photovoltaic cells that directly transform incident sunlight into electrical power.

This chapter presents an overview of solar energy. It introduces the fundamental principles of photovoltaic systems and the process of electricity generation based on the photovoltaic effect. In addition, it examines the variation of solar energy as a function of geographical location and seasonal conditions.

I.2. Overview and Motivation

Fossil fuel reserves are under a lot of strain due to the growing worldwide demand for electrical energy, which is mostly produced from fossil fuels like coal and oil. This has also had a major impact on the environment. Fossil fuels continue to be the primary energy source, but their limited supply leads to significant emissions of greenhouse gases, such as carbon dioxide (CO_2), methane (CH_4), and nitrous oxide (N_2O), which are major causes of climate change (IPCC, 2007).

Environmental problems are further exacerbated by the use of fossil fuels for transportation and the continuous growth of industrial operations, which have resulted in severe air pollution [1, 2] . It is essential to switch to alternate, sustainable, and clean energy sources in order to maintain economic growth while protecting natural ecosystems for future generations. International frameworks such as the Kyoto Protocol underline the need for coordinated global efforts to achieve these goals [3].

Renewable energy sources (RES) are being advocated more and more as a power generation alternative in response to these issues. Due to regulatory initiatives aimed at preventing climate change and guaranteeing a sustainable energy supply, the contribution of renewable energy to electrical grids has increased significantly over the past few decades (World Energy Outlook). As shown in Figure 1.1, RES made up more than 33% of the world's power generation capacity in 2023, indicating their growing importance in the energy mix [4]. In contrast to fossil fuels, renewable energy sources including wind, solar, biomass, and hydroelectric power generate electricity without releasing greenhouse gases, which helps to reduce air pollution and mitigate climate change.

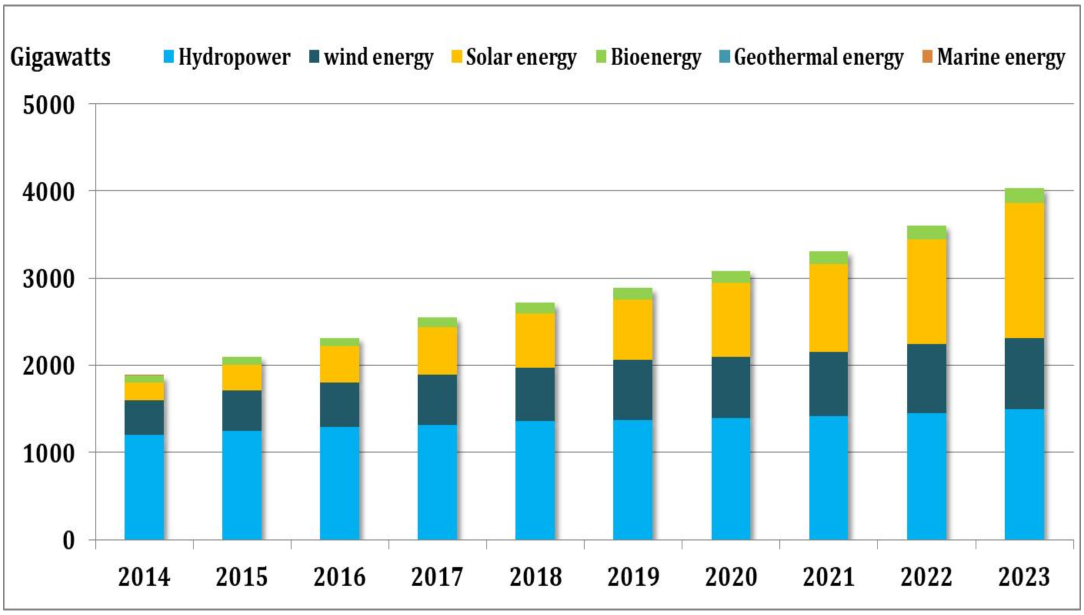

Figure I.1 : Global power generating capacity [4]

Wind power and solar photovoltaic energy have grown significantly among renewable energy technologies, surpassing other types of RES. Photovoltaic systems (PV) and wind power make up around 33% and 28% of new renewable energy installations, respectively, as Figure 1.2 illustrates. The potential of these technologies to take the lead in decarbonizing the energy sector is highlighted by this trend. In instance, the geographical potential for solar energy varies greatly by area, as Figure 1.3 shows.

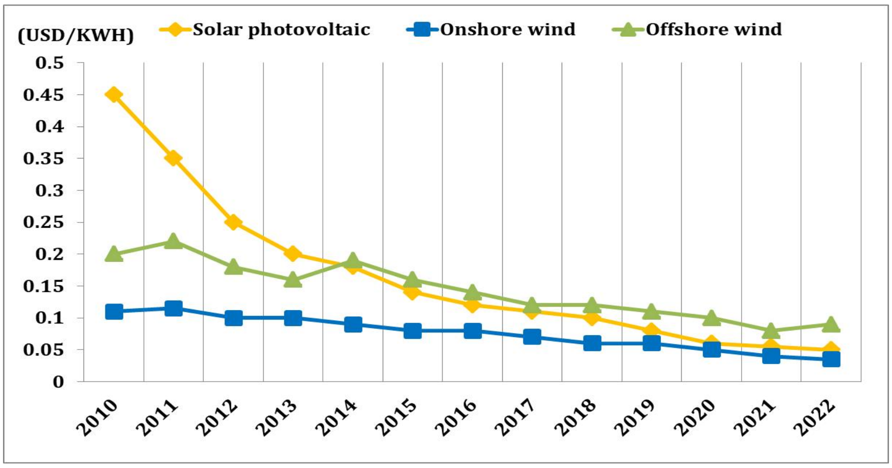

Figure I.2 Levelised cost of electricity from newly commissioned solar PV, onshore wind power and offshore wind power, 2010-2022 [5].

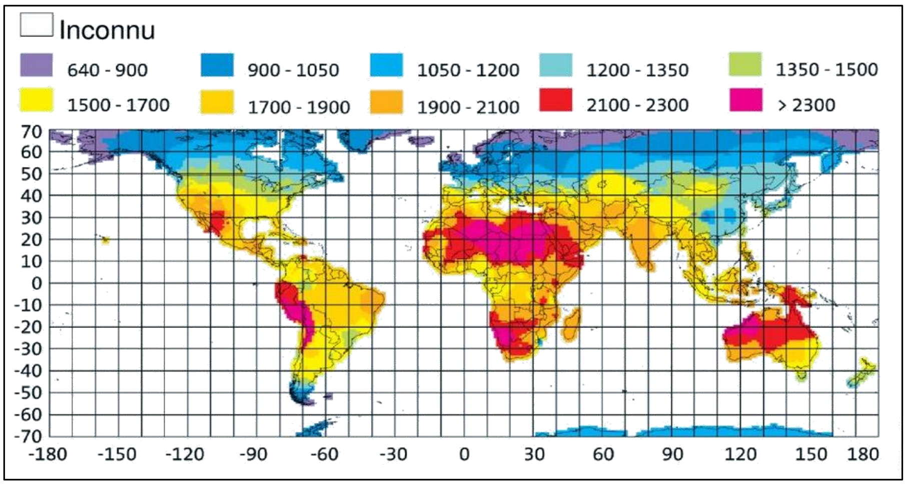

Figure I.3 : Solar irradiation map of the world from photovoltaic guidenr

Recent years have seen a significant decrease in the levelized cost of electricity (LCOE) related to renewable energy technology. With the global average LCOE falling by 50% between 2010 and 2022 to reach USD 0.033 per kilowatt-hour (kWh), onshore wind energy has shown the most notable decline among them. In a similar vein, solar photovoltaic (PV) systems have seen a notable decrease in cost; in 2022, the global average LCOE was recorded at USD 0.049 per kWh. On the other hand, with an LCOE of USD 0.081 per kWh, offshore wind energy is still relatively more expensive (see Figure 1.2).

Even with these improvements in cost-efficiency, the intermittent nature of renewable energy sources, especially solar PV, makes it difficult to integrate them into the power grid. Direct grid connection is not feasible because of the inherent variability of the direct current (DC) voltage output from these systems, which is impacted by changing climatic circumstances. Power electronic converters (PECs), a crucial technological answer, have advanced as a result of this difficulty.

Power electronic converters are devices that act as a bridge between the electrical grid and renewable energy systems. By dynamically controlling the output voltage, guaranteeing effective power conversion, and upholding a balanced power distribution, these converters mitigate output voltage variability. By performing these tasks, PECs improve grid compatibility and guarantee the dependable distribution of electricity produced from renewable sources.

I.3. Power Electronics Converters for Renewable Energy System

When integrating renewable energy sources (RES) with the electrical grid or load systems, power electronic converters (PECs) are crucial. Their operation has a significant impact on the system's overall performance, especially on elements like stability, dependability, efficiency, power quality, and consumption ratio.

To ensure energy conversion processes that are both cost-effective and efficient, various innovative Photo electrochemical (PEC) systems are being developed alongside the increasing practical implementation of renewable energy technologies [4]. Figure 1.4 presents a detailed framework for the integration of Renewable Energy Sources (RES) through the application of Power Electronic Converters (PEC). The incorporation of RES into electrical systems necessitates the deployment of PEC to align the outputs of RES with the requirements of the power grid. Consequently, significant advancements have been made in enhancing the efficiency of PEC systems. These improvements can be achieved through two primary approaches: (a) the development of novel power converter designs or (b) the implementation of advanced control strategies.

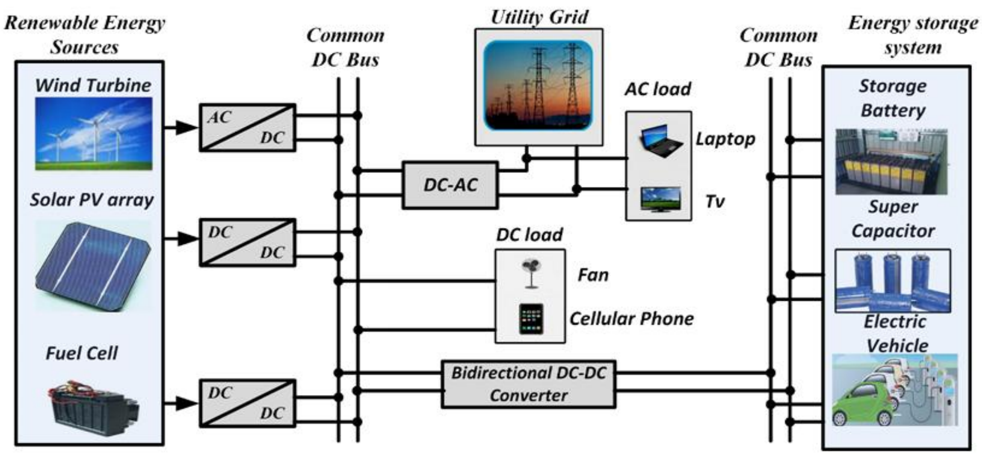

Figure I.4:. Schematic exhibiting the relationship of a RES to the electricity grid

The classification of converters in renewable energy systems (RES) encompasses two primary categories: galvanic ally isolated and non-isolated variants [6], [7]. Galvanically isolated converters, also known as transformer-based converters, employ a transformer to achieve input-output isolation, as highlighted in the topological analyses of [8],[9], [10]. This isolation mechanism enhances their functional potential. However, the inclusion of transformers introduces notable challenges, including increased financial costs, larger physical dimensions, and reduced operational efficiency. These limitations, absent in non-isolated or transformer-less solutions, are substantiated by empirical findings from case studies [11, 12]. Therefore, non-isolated converters emerge as a more favorable option in power conversion processes when all critical factors are considered.

I.3.1. Classification of power converters

For effective power conversion and energy conservation, power electronic converters have been utilized in numerous industrial applications. The following four categories can be used to classify power converters based on the type of electric power conversion and the electric power flow:

AC-DC rectifiers: Convert a single-phase or three-phase AC voltage to DC is used as front-end in variable-speed motor drives and wind energy conversion systems.

- **DC-DC converters:** Convert a DC voltage from one level and a certain polarity to a DC voltage of another level and in some applications to another polarity.
- **DC-AC inverters:** Conversion from DC to variable-voltage and variable-frequency AC is used invariable-speed motor drives. Conversion of unregulated or regulated DC to fixed AC is used in grid-connection of renewable energy sources.
- **AC-AC cycloconverters:** Convert an AC voltage of one level, frequency and number of phases to an AC voltage of a different level, frequency, and in some applications to different number of phases.

I.3.2. Review of PV Energy System Applications

Photovoltaic (PV) energy conversion systems play a crucial role in the integration of renewable energy into the utility grid, providing a sustainable and efficient solution for electricity generation. Figure 1.5 illustrates the structural configuration of such a system, beginning with PV arrays that harvest solar irradiance and convert it into direct current (DC) electrical energy, which is subsequently stabilized via DC bus structures. A multilevel power electronics converter serves as the pivotal component, facilitating the conversion of DC power into alternating current (AC) power characterized by high quality and reduced Total Harmonic Distortion (THD). A filtering stage ensures compliance with grid standards by attenuating high-frequency noise, while an optional transformer is incorporated to perform voltage adaptation and provide electrical isolation between the PV system and the grid. The control unit, incorporating a Maximum Power Point Tracking (MPPT) controller, ensures optimal energy harvesting from the PV arrays and precise regulation of the power electronics converter. Ultimately, the AC power is injected into the utility grid, demonstrating a sophisticated integration of advanced control algorithms and power conversion technologies for efficient solar energy utilization and grid compatibility.

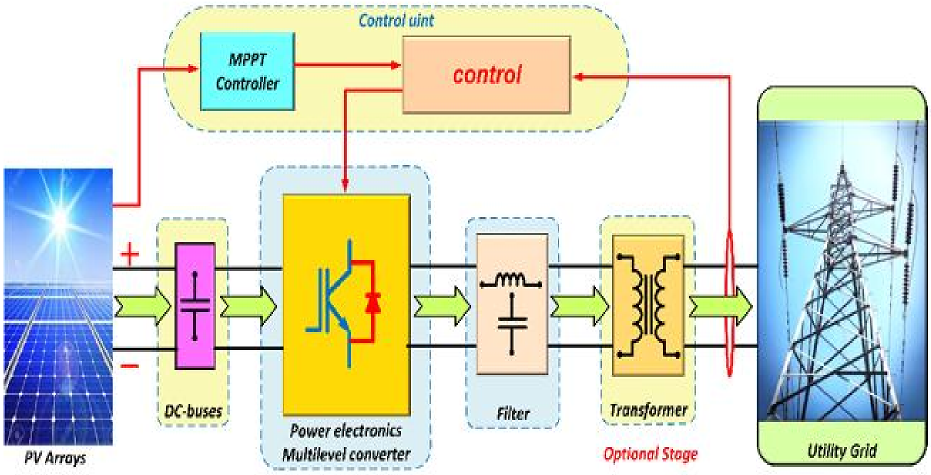

Figure I.5.A photovoltaic (PV) system with power electronics and the needed control

I.3.3. Classification of DC–DC converters

In order to increase efficiency and overcome the drawbacks of converters, numerous researchers have studied various DC-DC converter types for storage and renewable energy applications. Figure 1.6 [13–15] illustrates how DC–DC converters are divided into three main technologies according to how they operate. They are hard switching mode, gentle switching mode, and linear mode. Features of the linear mode include simplicity, fast response, and low noise with effective regulation. However, its disadvantage is low efficiency because of power losses under different operating situations. Based on galvanic isolation, hard switching mode converters can be further divided into isolated and non-isolated converters. Hard switching mode topologies that lack galvanic isolation (non-isolated) and are referred to as chopper circuits include the buck, boost, buck–boost, and Cuk converters. However, when the converters are powered by the utility grid, galvanic isolation (transformer) is required for safety reasons. With their control strategies, power converters (PCs) assist in controlling the voltages of microgrid nodes with a variety of loads, including resistive, inductive, nonlinear, constant power, and critical loads. However, constant power loads (CPLs) have an impact on PC output voltage stability and are typically challenging to control using conventional control methods [16, 17].

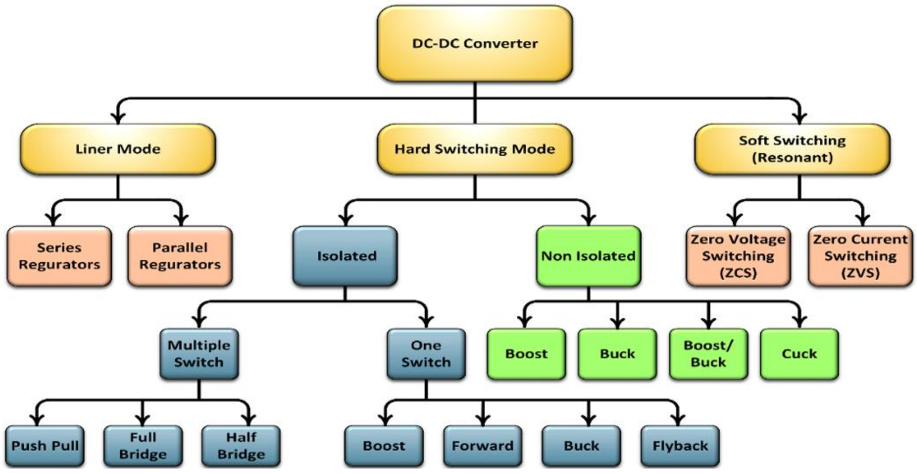

Figure I.6 : Classification of DC – DC converters[18]

I.4. Solar Radiation :

Solar radiation encompasses the totality of radiative emissions produced by the Sun. Alongside cosmic rays particles distinguished by extremely high velocities and energies the Sun releases electromagnetic radiation spanning a broad spectrum, from radio waves to gamma rays, including the visible region.

The Sun's electromagnetic emission can be accurately represented by a blackbody model at a temperature of approximately 5800 K, in accordance with Planck's law. The maximum of the emission spectrum lies within the yellow region (λ = 570 nm), with the energy distribution being approximately equally divided between the visible and infrared ranges, while about 1% lies in the ultraviolet domain. After propagating through the Earth's atmosphere and reaching sea level, solar radiation is subjected to several filtering processes. These are evidenced in the spectrum by absorption bands attributed notably to ozone which absorbs a substantial fraction of ultraviolet radiation as well as oxygen, carbon dioxide, and other atmospheric constituents [19].

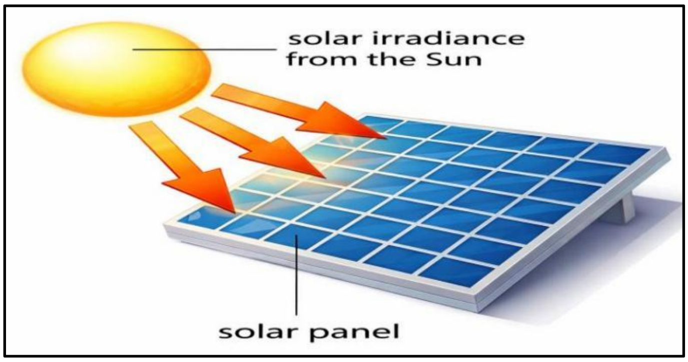

Figure I.7 : Representation of Solar Radiation

I.4.1. Radiation Spectrum:

The notion of solar energy may initially appear abstract; however, it fundamentally corresponds to the heat and light naturally emitted by the Sun. The development of photovoltaic cells during the previous century enabled the utilization of this resource to supply energy for modern civilization. Through photovoltaic solar panels, incident light energy is directly converted into an electrical current.

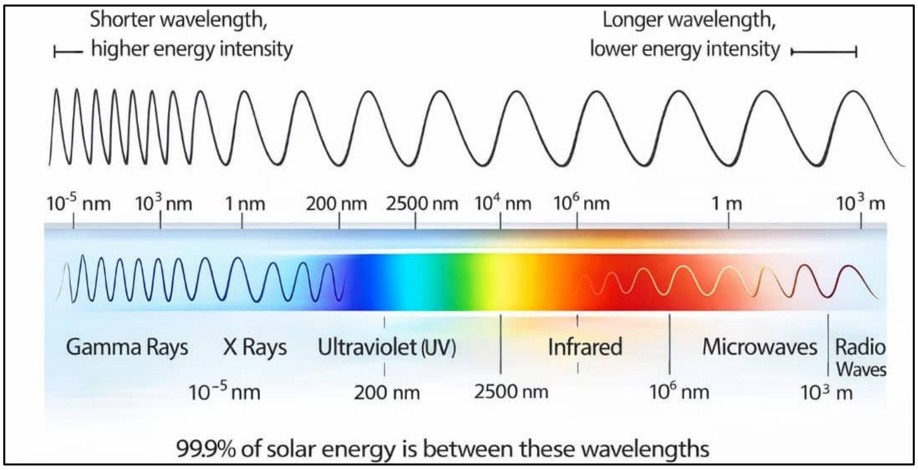

Figure I.8 : Solar Radiation Spectrum

Although the electromagnetic spectrum covers a broad range, approximately 99.8% of the Sun's radiant energy is concentrated within a relatively narrow wavelength interval extending from 20 to 2500 nanometers. Only a limited portion of this solar radiation reaches the Earth's surface, ranging from radio waves with wavelengths of several decameters to the longest ultraviolet rays, while the remaining radiation is either reflected or absorbed by the atmosphere and the ionosphere [20].

Figure (1.9) presents the solar radiation spectrum. The spectral distribution of solar energy consists of approximately 5% ultraviolet radiation, 42% visible light, and 53% near-infrared radiation

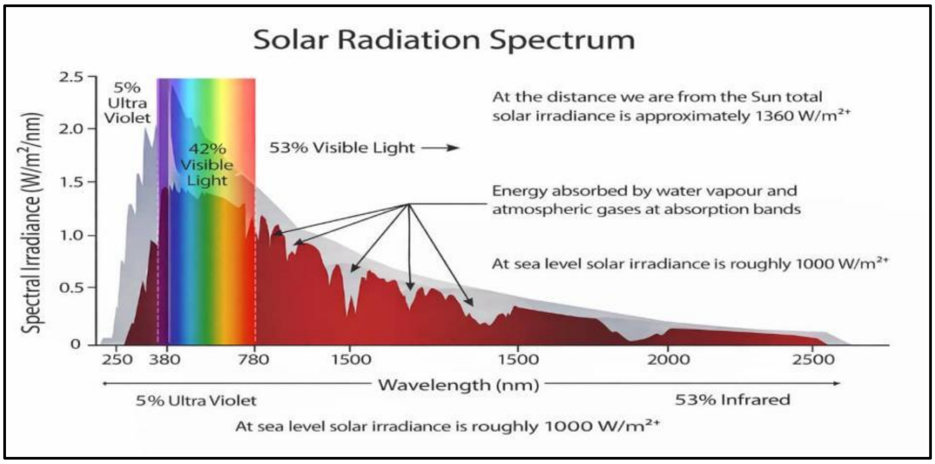

Figure I.9 : Representation of Solar Radiation Spectrum

I.5. Conversion of Solar Radiation by PV Effect:

A photovoltaic (PV) cell is composed of two silicon layers that are intentionally doped to establish electrical polarization. One layer is rendered positive (P-type) through the incorporation of boron atoms, while the other is made negative (N-type) by introducing phosphorus atoms, resulting in the formation of a potential barrier at their junction. When a photon possessing sufficient energy is absorbed by the semiconductor material, it disrupts a valence bond and liberates an electron, simultaneously generating a positively charged hole. This phenomenon, known as the photovoltaic effect, gives rise to a potential difference between the two layers. When the layers are electrically connected, electrons flow from one region to the other, thereby producing an electric current [19].

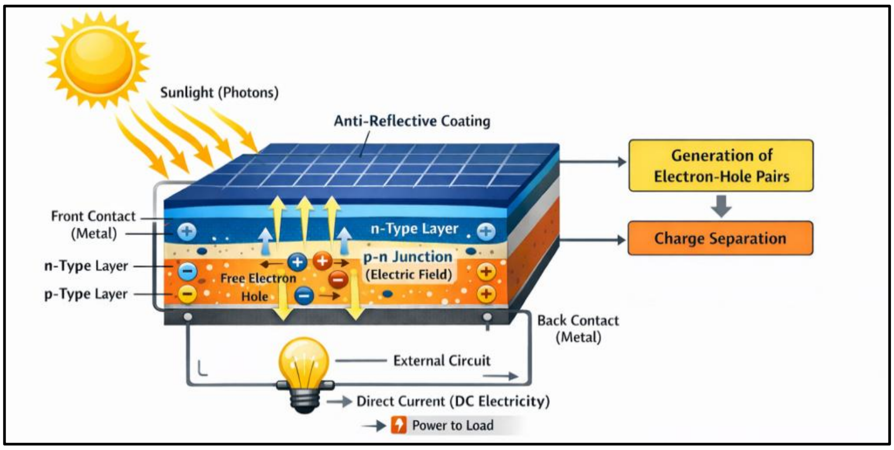

Figure I.10: Solar Radiation Conversion by PV Effect

I.6. Photovoltaic Generator:

The electrical characteristics of the photovoltaic sensor, specifically the relationship between current and voltage (I=f(V)), are depicted in Figure (1.11).

Using two input variables,temperature and the illumination the sensor receives,this modeling is frequently used to estimate the sensor output (voltage, current).

The photovoltaic module's current output at a specific voltage is solely dependent on the cell's temperature and light. The load in the electrical circuit affects a solar cell's efficiency when the temperature and illumination are constant. In an open circuit configuration (Rc = ∞, I = 0, V = Voc) or a short circuit (Rc = 0, I = Icc, V = 0), no energy is transmitted outside. Between these two extremes, an optimal value Ropt of the load resistance Rc exists, for which the power

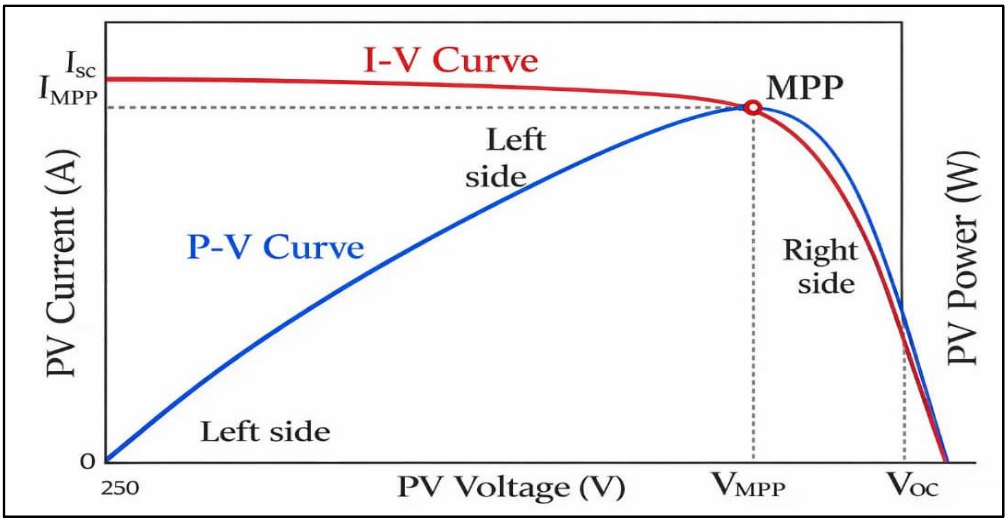

Figure I.11: Typical Characteristics of a PV Generator

(P=Vmax × Imax) provided by the solar cell to the load resistance is maximal, thus reaching Pmax [20].

The formula for the solar cell's energy efficiency is $\eta = P/P\gamma$, where $P\gamma$ is the incident light power on the cell's surface. The solar cell's efficiency reaches its maximum at the ideal value R opt of the load resistance Rc, and $\eta max = Pmax/P\gamma$. The spectrum of the incident radiation and the junction temperature determine the value of Ropt, which is not a characteristic constant for a particular cell. In actuality, efficiency declines with temperature, which occasionally prompts the development of hybrid sensors that combine a solar cell and a thermal sensor.

The material and manufacturing technology (amorphous silicon, polycrystalline silicon, monocrystalline silicon), the junction geometry (layer thickness, multilayers, etc.), and external factors (temperature, spectrum and power of the incident radiation, external electrical circuit connected to the cell, etc.) all affect the power and efficiency of the solar cell ($P=I\times V$)

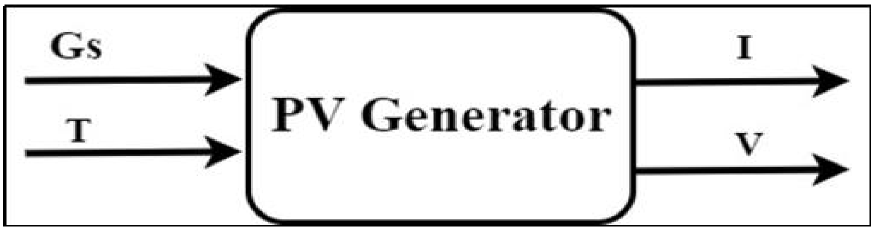

Figure I.12: Block Diagram of a PV Generator

I.6.1. Photovoltaic Cell:

An arrangement of connected solar cells makes up photovoltaic modules. These resin-embedded cells are enclosed either between a glass pane and a Tedlar sheet (glass/Tedlar module) or between two tempered glass panes (double-glass modules). Although frameless modules are available for building integration applications using aluminum profiles on facades or roofs, this assembly is usually placed into an anodized aluminum frame. A module's highest power for a reference maximum solar irradiation of 1000 W/m² is represented by peak watts (Wp), which are determined by the module's surface area and incident solar irradiation.

An arrangement of connected solar cells makes up photovoltaic modules. These resin-embedded cells are enclosed either between a glass pane and a Tedlar sheet (glass/Tedlar module) or between two tempered glass panes (double-glass modules). Although frameless modules are available for building integration applications using aluminum profiles on facades or roofs, this assembly is usually placed into an anodized aluminum frame. A module's highest power for a reference maximum solar irradiation of 1000 W/m² is represented by peak watts (Wp), which are determined by the module's surface area and incident solar irradiation.

The voltage output of a module is related to the number of cells wired in series. For modules with lower power (less than 75 Wp), the voltage usually stays in the 12 to 15 volts range. We can get higher power modules by putting more cells in series to raise the voltage. Also, adding more cell branches in parallel raises the current. Depending on the needs of the system, the voltage can then be 24 volts or higher. Module surface area changes between producers, but it is usually between 0.5 and 1 square meter. For custom builds, it can reach 3 square meters. Several interconnected modules create a panel, and several panels together create a photovoltaic array. By connecting modules in series or parallel, we can make different voltages and power levels [19].

I.6.2. Modelling of a PV Cell:

The working of a photovoltaic module can be shown by using the standard one-diode model. Shockley created this model for a single photovoltaic cell. It was then made more general for a photovoltaic module by thinking of it as many similar cells wired in series or parallel.

In papers, a photovoltaic cell is often seen as a current generator that acts like a current source with a diode across it. To explain cell-level physics, the model adds two resistances, Rs and Rsh, as seen in the circuit diagram in Figure (1.13).

The series resistance is the cell's internal resistance. It mainly depends on the resistance of the semiconductor used, the contact resistance of the collecting grids, and how resistive these grids are. The shunt resistance comes from leakage current at the junction, which depends on how the cell was made

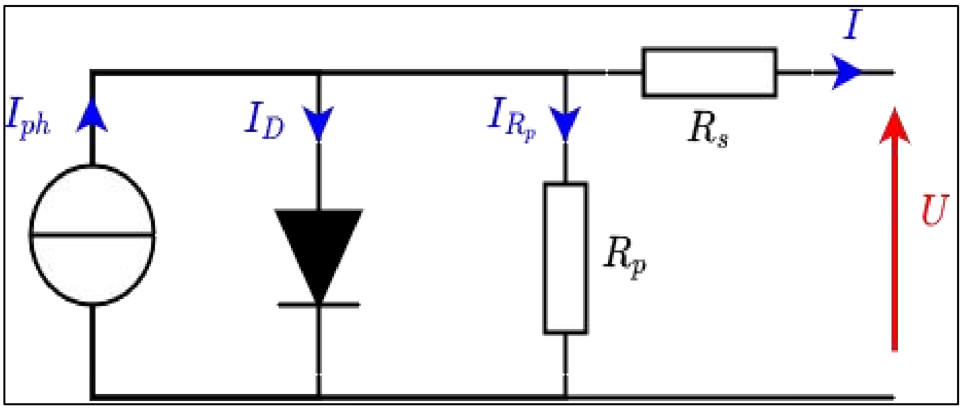

Figure I.13: Equivalent Circuit of a PV Cell

I.6.3. Types of Photovoltaic Cells :

Photovoltaic solar panels consist of photovoltaic cells, which differ based on their type:

(1) Mono crystalline Cells: These cells are created by cooling molten silicon, which then solidifies into a consistent crystal. This crystal is sliced into thin pieces to make the photovoltaic cell. The material is typically blue and free from visible crystals or impurities.

Figure I.14: Monocrystalline Cells

(2) Poly-crystalline Cells: These cells are made by melting silicon in a square metal mold, called an ingot. The cells appear blue with speckled patterns left by the crystals, making them easy to identify.

Figure I.15: Polycrystalline Cells

(3) Hydrogenated Amorphous Cells: Amorphous silicon is produced from silicon gas that is vaporized onto a support like glass, flexible plastic, or metal through vacuum deposition. These cells are usually dark gray.

Figure I.16: Hydrogenated Amorphous Cells

I.7. The Impact of Temperature on Solar Panel:

The performance of solar panels is greatly impacted by temperature. Here's how:

• **Reduction in Efficiency:** Solar panels lose efficiency as their temperature rises. The process by which solar panels generate power from sunlight becomes less efficient as the temperature rises.

• **Voltage Decrease:** When a solar panel's temperature rises, its voltage falls. This is because as the temperature rises, the semiconductor material used in solar panels loses some of its ability to transfer charges.

• **Power Output Reduction:** As temperatures rise, solar panels may produce less power. This is due to the fact that the overall power production is adversely affected by the decline in efficiency and voltage.

• **Thermal Degradation:** Over time, high temperatures can lead to thermal degradation of solar panel materials, which shortens their lifespan and decreases their efficiency.

• **Operating Temperature Range:** Solar panels are made to function in a specific range of temperatures. The panels' performance may be further hampered if temps rise over this range.

As temperatures rise, solar panels' efficiency declines, affecting their overall performance and output, even if they can still produce power on hot days.

I.8. Advantages and Disadvantages of PV Energy:

I.8.1. Advantages:

- **Renewable Energy**: Solar energy is a long-term, sustainable energy source since it is a plentiful and readily accessible renewable resource.
- **Low Greenhouse Gas Emissions**: Using solar energy helps to prevent climate change by lowering carbon emissions because it doesn't emit greenhouse gases.
- **Decreasing Costs**: Over time, the price of solar technology has dropped dramatically, making solar energy more affordable than traditional energy sources.
- **Energy Independence**: By enabling customers to generate their own electricity, photovoltaic systems lessen reliance on energy providers and changes in market prices.

- **Low Maintenance**: After installation, solar installations require little upkeep, which lowers long-term maintenance expenses.

I.8.2. Disadvantages:

- **Sunlight Variability**: Because solar energy is dependent on the amount of sunlight, photovoltaic electricity generation is erratic and sporadic, frequently necessitating energy storage or integration with other energy sources.
- **High Initial Costs**: Initial investments in solar systems can still be somewhat substantial, even though the costs of solar technology have fallen.
- **Environmental Impact**: While solar energy is generally considered clean, the manufacturing and disposal of solar panels can have an environmental impact.
- **Space Requirement**: In order to fit solar panels, solar installations frequently need sizable land or roof surfaces, which might present difficulties in crowded cities or places with little space.
- **Dependency on Weather Conditions**: At some times, weather conditions like clouds, rain, or snow can lower the efficiency of solar electricity production.

I.9. Conclusion:

In conclusion,The principles of solar radiation and photovoltaic energy conversion were discussed in this chapter. It described how solar cells use sunlight to create electricity by utilizing the photovoltaic effect. The modeling and characteristics of photovoltaic generators were discussed, including factors influencing their efficiency like temperature and load resistance. A variety of silicon crystal-based photovoltaic cell types were showcased. The chapter also touched upon the components of photovoltaic modules and highlighted the key advantages and disadvantages of solar photovoltaic technology.

Chapter II

Modeling and control of photovoltaic systems

II.1. Introduction

With the increasing demand for renewable energy, photovoltaic (PV) systems have emerged as a significant means of generating sustainable power. However, integrating these systems into the electrical grid requires accurate modeling, effective control strategies, and efficient power conversion techniques to ensure their reliability and optimal performance.

This chapter provides an overview of the key components involved in grid-connected PV systems. It emphasizes elements such as DC-DC converters, maximum power point tracking (MPPT), voltage source inverters (VSIs), and grid synchronization methods. Each component plays a critical role in enhancing energy conversion efficiency and maintaining power quality.

The discussion begins with a summary of PV system modeling approaches, followed by an examination of DC-DC converters and their function in voltage regulation. Subsequently, MPPT algorithms are reviewed to illustrate their contribution to optimizing energy extraction from solar panels. The chapter then addresses the control of VSIs, which are essential for converting DC power to AC and ensuring a stable interface with the grid. Lastly, the principles of grid synchronization are outlined, highlighting mechanisms that support continuous operation within the power network.

II.1.1. Grouping cells in series

A single photovoltaic cell produces a small amount of power, which isn't enough for most home or factory uses. So, to make more powerful photovoltaic generators, many cells are linked together in series or parallel arrangements.

When cells are connected in series, the generator's voltage goes up. The same current flows through each cell, and the total voltage is the sum of each cell's voltage, as shown in Figure II.1.

Equation (1.3) summarizes the.electrical characteristics.of a series.connection of (Ns) cells:

$$V_{oc_{N_s}} = N_s \times V_{oc}; I_{cc_{N_s}} = I_{cc} \qquad \text{II.1}$$

$V_{oc_{N_s}}$: The sum of the.open-circuit.voltages of the (Ns) cells in series.

$I_{cc_{N_s}}$: The short-circuit.current of the (Ns) cells in series.

This connection.system is generally.the most commonly.used for.commercial.photovoltaic modules.

As the surface.area of the.cells increases, the.current produced.by a single cell steadily increases with technological advancements, while its.voltage remains very.low. The.series connection thus allows.for an increase.in the overall.voltage, thereby.enhancing the total power.output.

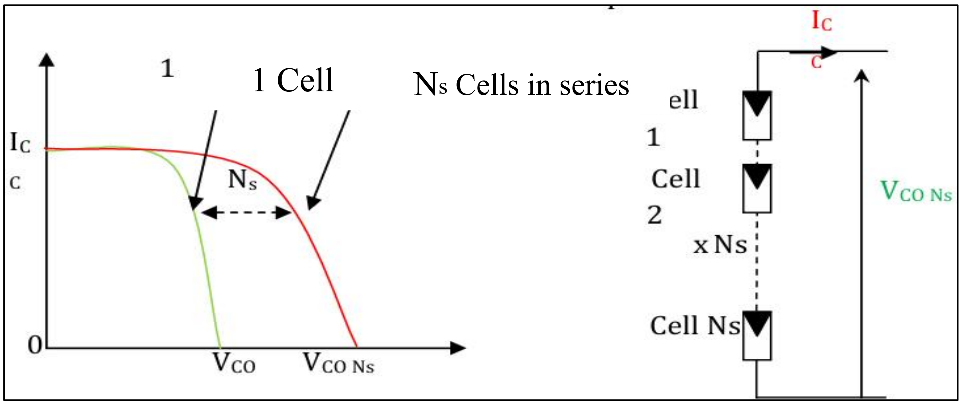

Figure II.1: Resulting characteristic of a series connection of (Ns) cells.

II.1.2. Parallel Connection of Cells

A parallel.connection of (Np) cells is.possible and allows.for an increase in the output current of the generator.thus created. In a grouping.of identical.cells connected.in parallel, the cells are subjected to the same.voltage, and the.resulting characteristic.of the grouping is obtained by adding the.currents.

Figure II.2 summarize the .electrical characteristics. of a parallel connection of (Np) cells.

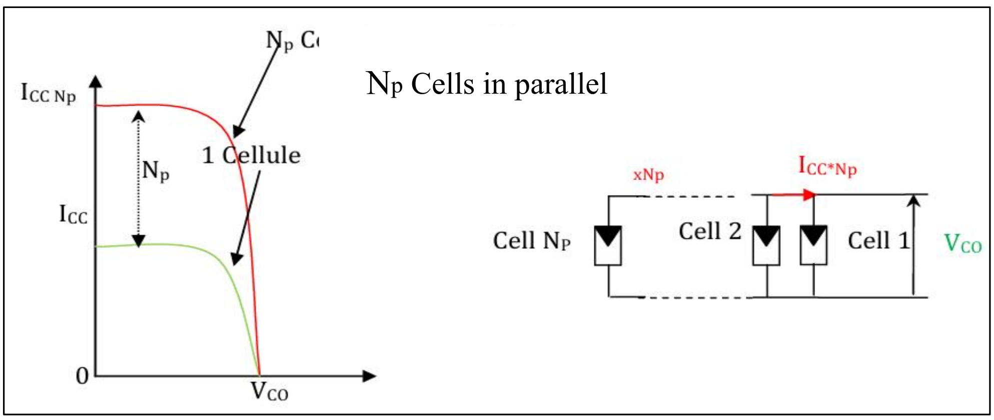

Figure II.2: Resulting characteristic of a parallel connection of (Np) cells [19, 20].

$$I_{cc_{N_p}} = N_p \times I_{cc} \quad \text{II.2}$$

$$V_{oc_{N_p}} = V_{oc} \quad \text{II.3}$$

$I_{cc_{N_p}}$: The sum of the. short-circuit currents .of (Np) cells .connected in parallel.

$V_{oc_{N_p}}$: The open-circuit.voltage of (Np) cells.connected.in parallel.

II.1.3. Hybrid Connection of Cells (Series & Parallel)

Depending on the.series and/or parallel.connection of these.cells, the values.of the total.short-circuit current and the.total open-circuit.voltages are.given by.the following.relations:

$$I^t{}_{cc} = N_p \times I_{cc} \quad \text{II.4}$$

$$V^t{}_{oc} = N_c \times V_{oc} \quad \text{II.5}$$

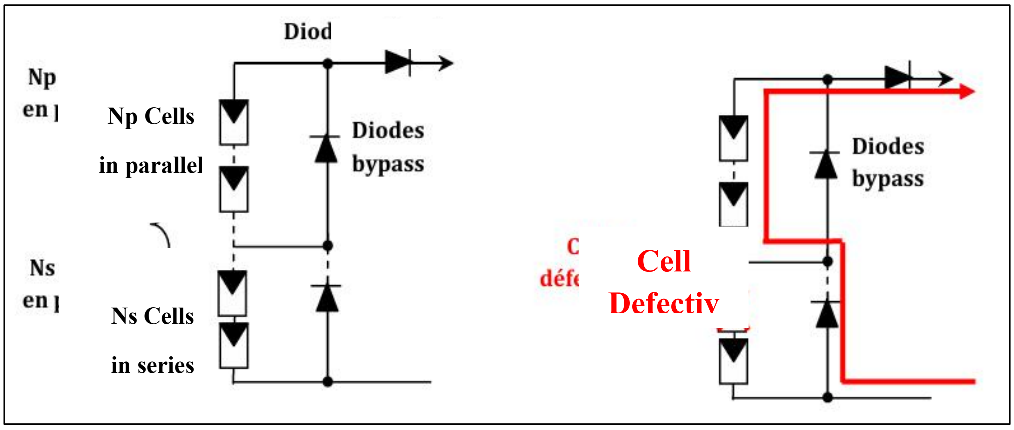

Figure II.3: Resulting characteristics of a hybrid connection of(Ns x Np) cells [19, 20] .

Where:

N_c: Number of.cells connected.in. parallel.

N_p: Number of.cells connected. in series.

$I^t{}_{cc}$: Total.short-circuits. current.

$V^t{}_{oc}$: Total .open-circuit. voltage.

Thus, the characteristic Ip Vp of a photovoltaic.generator can be.considered the result of a network of Ns x Np cells connected.in series/parallel. The.overall characteristic.can also vary depending.on illumination, temperature, cell aging, shading.effects, or illumination.inhomogeneity. Furthermore, even single.shading or.degradation of a.cell in a series.connection can cause a significant reduction in the.current produced by.the photovoltaic module.

When a cell that isn't getting much light draws more current than it makes, its voltage goes negative, and it starts acting like a load. This can cause it to waste too much power, which could ruin it if the problem lasts. This is called the hot spot effect.

To fix this, solar panels use bypass diodes. They keep cells that go passive safe. When a bypass diode turns on, it shorts out part of the panel, stopping reverse currents in bad cells. This fix lowers both the power output and the voltage at the panel's ends. If a cell goes bad, the group of cells linked to it and protected by the bypass diode can't make power anymore.

When a module experiences a single cell failure without protective measures, the result, a complete power loss, calls for comparison with the partial power reduction seen in this event.

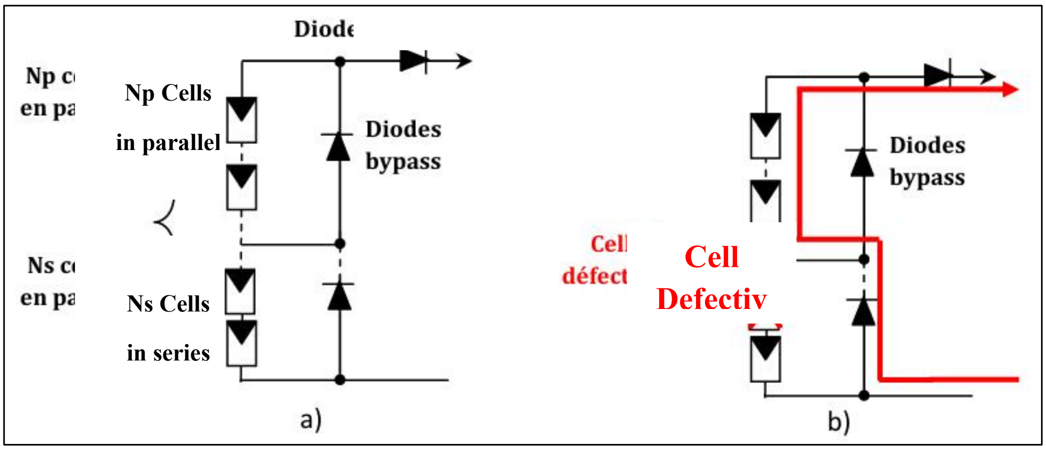

Figure II.4: a) Classical architecture.of a photovoltaic module.with protective diodes

b) Failure of one of the PV.module cells and activation of the bypass diode, highlighting the circulation current .

II.2. Modeling of Photovoltaic Installation Elements

II.2.1. Conversion of Light into Electricity

Photovoltaic generators change light into electricity through semiconductor devices known as photovoltaic cells, often made of silicon [21].

A photovoltaic generator, also called a solar field, has photovoltaic panels linked in series and/or in parallel to get the needed power. These panels sit on a metal frame that holds the solar field at a certain angle.

The photovoltaic panel has cells in series and cells in parallel, covered by glass. Putting cells in series raises the voltage for a given current, while parallel ties raise the current while keeping the voltage the same.

II.2.2. Two-Diode

The two-diode.model includes an additional diode for better curve fitting. This diode represents the phenomenon of recombination.of.minority carriers, both on the.surface of the material and within its.volume.

This model appears.more sophisticated.and provides greater.precision but is.somewhat.complex and.challenging to solve. It.requires.knowledge of four parameters.under standard sunlight and temperature.conditions. These.parameters are.generally.provided by the manufacturer.or can be obtained.through.module testing.fewer than three.conditions: short-circuit.current (Icc), open-circuit.voltage (Voc), maximum.voltage (Vmax), and.maximum current ($Imax$) at.the point of maximum.power.

Temperature.coefficients are also.necessary in this.modeling technique to.account for the effect of temperature.on the critical.parameters of.the solar cell.

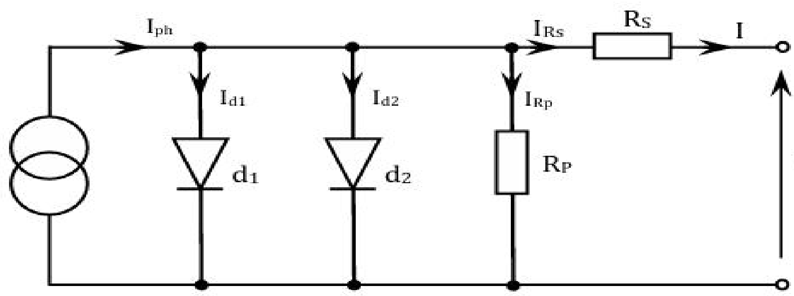

Figure II.5: Electrical two-diode equivalent model of a photovoltaic cell.

$$I_{d1} = I_{s1}\left[e^{\frac{q(V+IR_s)}{n_1kT}} - 1\right]$$

II.12

Avec :

$$I_{d2} = I_{s2}\left[e^{\frac{q(V+IR_s)}{n_2kT}} - 1\right] \qquad \text{II.13}$$

Ainsi :

$$I_{ph} = I + I_{d1} + I_{d2} + I_{Rp} \qquad \text{II.14}$$

$$I = I_{ph} - I_{d1} - I_{d2} - I_{Rp}$$

Alors :

$$I = I_{ph} - I_{s1}\left[e^{\frac{q(V+IR_s)}{n_1kT}} - 1\right] - I_{s2}\left[e^{\frac{q(V+IR_s)}{n_2kT}} - 1\right] - \frac{V + IR_s}{R_p} \qquad \text{II.15}$$

n1 , n2 : Ideality.factors of diodes d1 and d2 (ranging.between 1 and 2, depending.on the technology).

The photocurrent.depends on the.temperature, and its.expression is:

$$I_{ph}(T) = I_{ph}(T = 298K)\left[1 + (T - 298K) \cdot (5 \cdot 10^{-4})\right]$$

I_{s1}, I_{s2}: These are.the saturation.currents of diodes d1 and d2, respectively, and . they depend on the.temperature:

$$I_{S1} = K_1 T^3 e^{\frac{-Eg}{KT}} \qquad \text{II.16}$$
$$I_{S2} = K_2 T^{\frac{5}{2}} e^{\frac{-Eg}{KT}}$$

Where:

Eg: Energy, with

*K*1=1.2A/cm2 *T*3K1 and *K*2=2.9×105A/cm2 *T*5/2.

For a solar.panel consisting of z cells.connected in series, and.considering the.model in Figure II.6, the.equation.describing.this panel is:

$$I = I_{ph} - I_{s1}\left[e^{\frac{q(V+IzR_s)}{zn_1kT}} - 1\right] - I_{s2}\left[e^{\frac{q(V+IzR_s)}{nz_2kT}} - 1\right] - \frac{V + IzR_S}{R_p} \qquad \text{II.17}$$

The Three-Diode.Model: The.third diode.is included.in the.equivalent.schematic to account for effects.not considered.in the other.models (e.g., leakage current related to the diodes).

The current.and voltage.across the terminals.of a photovoltaic.panel are.given by:

$$I_P = N_{cp} I_c \qquad \text{II.18}$$

$$V_P = N_{cs} V_c$$

Whereas the current and voltage across the terminals of a photovoltaic generator are given by:

$$I_g = I_{Pv} = N_{pp} I_P = N_{pp} N_{cp} I_c \qquad \text{II.19}$$
$$V_g = V_{Pv} = N_{ps} V_P = N_{ps} N_{cs} V_c$$

The current generated.by the photovoltaic.generator at a.given voltage.depends solely on the illumination.and the temperature.of the cell.

II.2.3. Single-Diode Model

The characteristic (I-V) of an elementary.cell is modeled by.the equivalent.circuit represented in Figure II.5. This circuit includes.a current source.and a diode.in parallel, as well.as series resistance. (Rs) and parallel (shunt) resistance (Rsh), to account.for dissipative phenomena.at the cell level [20, 23].

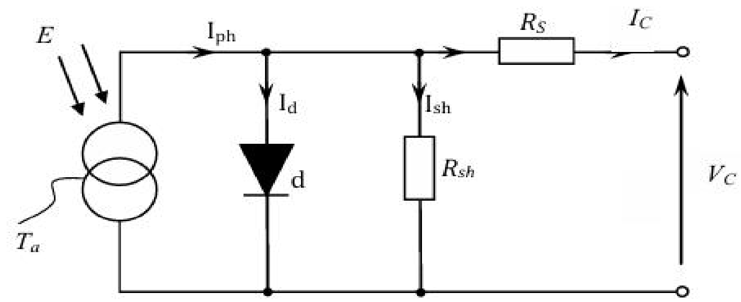

Figure II.6: Equivalent electrical schematic.of the PV cell with.a single diode.

With:

I_c : Current delivered by the cell.

I_{ph}: Photocurrent.generated by the.cell (proportional to the.incident.radiation)

I_d: Current of the diode.

I_{sh}: Shunt current.

$$I_{ph} = P_1 \cdot E_G \cdot \left[1 + P_2 \cdot (E_G - E_{\text{ref}}) + P_3 \cdot \left(T_j - T_{\text{jref}}\right)\right] \quad \text{II.6}$$

$$T_j = T_a + E_G \left(\frac{N_{oct} - 20}{800}\right) \quad \text{II.7}$$

$$I_d = I_s \left[\exp\left(\frac{q}{A \cdot K \cdot T_j}\left(V_c R_{s-p} \cdot I_c\right)\right) - 1\right] \quad \text{II.8}$$

$$I_s = P_4 \cdot T_j^3 \exp\left(\frac{-E_G}{K \cdot T_j}\right) \quad \text{II.9}$$

$$I_{sh} = \frac{V_c}{R_{sh}} \quad \text{II.10}$$

$$I_c = I_{ph} - I_d - I_{sh} \quad \text{II.11}$$

With:
EG: Solar irradiation.

$P1$, $P2$, $P3$, $P4$: Constants dependent on the nature of the cell material, determined experimentally by the manufacturer.

Ta: Ambient.temperature.

Tref: Reference temperature (298 K).

Tj: Temperature.of the cell.

Noct : Nominal.operating temperature of the.solar cell, as provided by the.manufacturer (45°C).

Eef: Reference.illumination (1000 W/m²).

Is: Saturation.current of the diode.

Eg: Energy gap for crystalline silicon (1.12 eV).

A: Ideal factor of the junction ($1 < A < 3$).

R_{sp}: Series resistance.of a photovoltaic panel.

R_{sh-p}: Equivalent resistance of a.photovoltaic panel.

q: Electron.charge (1.6×10^{-19} C).

K: Boltzmann constant (1.38×10^{-23} J/K).

Vc: Voltage across the.cell terminals.

II.2.4. Simulation results

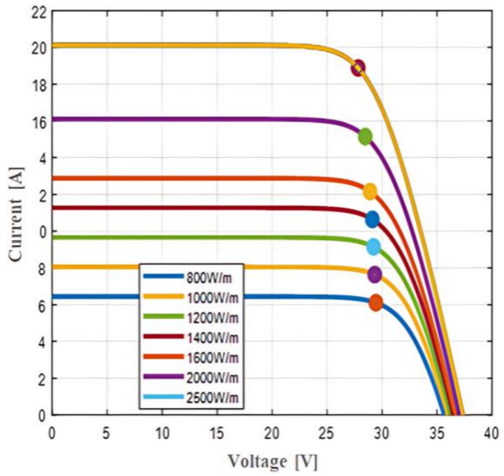

Figure II.7: I-V characteristics, variation of irradiance at constant temperature

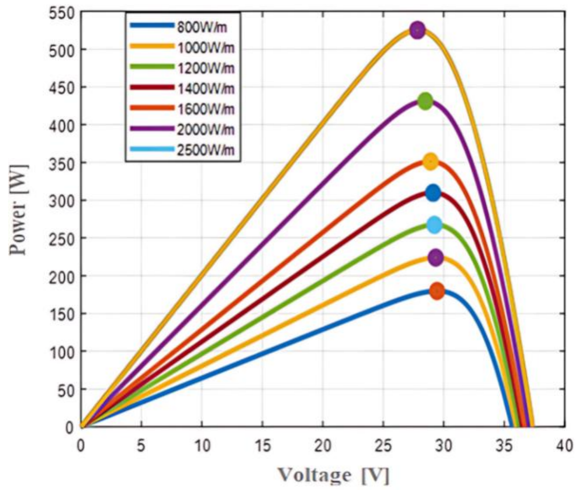

Figure II.8: P-V characteristics, variation of irradiance at constant temperature.

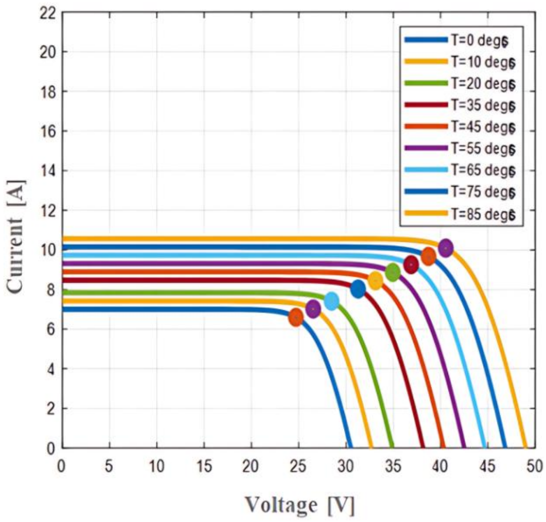

Figure II.9: I-V characteristics, temperature variation at constant solar radiation.

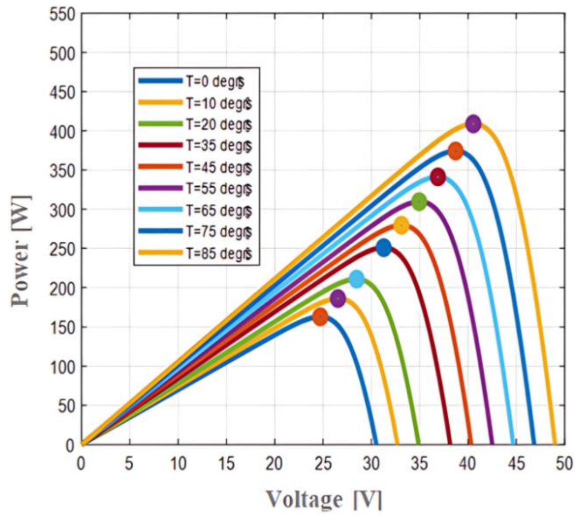

Figure II.10: P-V characteristics, temperature variation at constant solar radiation

A solar panel's performance is very sensitive to changes in light and temperature because these factors greatly change how much power the panel makes. Figure II.7 shows how current and voltage change with voltage at different light levels, while the temperature is held at 25°C. The figure shows a few power curves with the highest power points. Figure II.8 shows that both the open circuit voltage and short circuit current change at the same rate as the light level. In Figure II.9, when the light is constant (1000) and the temperature goes up, the open circuit voltage goes down, but the short circuit current stays about the same. So, how a solar panel works mainly depends on the environment around it. It's important to keep these things in mind when figuring out what size solar panel system is needed to get the power output you want.

Figures II.7 and II.8 show the effect of light on a solar panel through I-V and P-V curves, with the light ranging from 100 to 1000 at a steady 25°C. The current is steady as voltage goes up to 30 V, then it starts to drop. Also, the current goes up with stronger light, which proves that light has a big impact on the short circuit current. On the other hand, the open circuit voltage barely changes. The power performance curves confirm where maximum power can be found.

Looking at the figure, when the temperature changes from 0 to 80°C, it's clear that higher temperatures cause a drop in power as voltage changes.

II.3. factors and phenomena affecting the efficiency of photovoltaic cells module

II.3.1. Dust

The data shows how outside conditions impact how well solar panel systems work. Graph A shows how humidity affects voltage and power. As voltage goes up, power rises until it hits its highest point at about 13 V and 45 W. After that, power drops quickly, which means the system is not working as well. This could be due to humidity changing how well parts conduct electricity or how well they work overall. Graph B shows how dust affects current and voltage. Current stays about the same until a certain voltage, which is where the system works best. Then, it starts to go down slowly before dropping sharply after the highest voltage is reached, which shows that dust has a clear, bad impact. This is because dust can block some of the light or make it scatter oddly, which lowers the amount of electricity made and how well it is converted. Because of this, it is good to clean and care for the system often to make it work better.

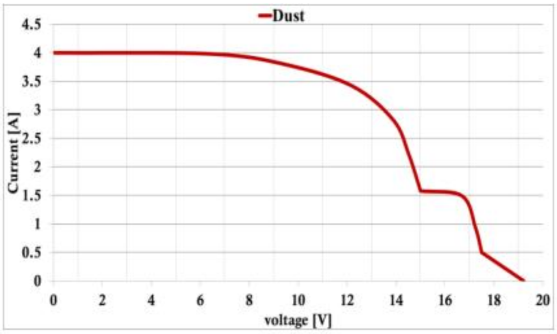

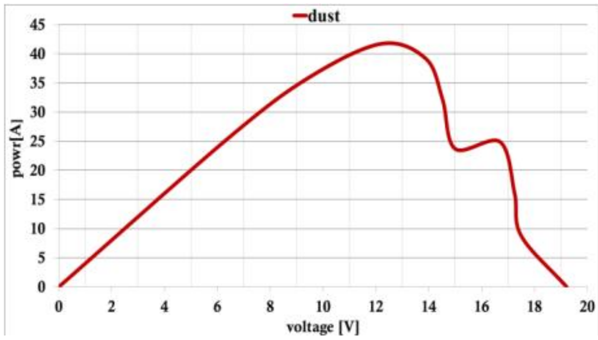

Figure II.11: shows the impact of dust accumulation on the PV panels. I-V curves below radiation levels show a reduction in current output and obvious distortion, emphasizing the importance of regular maintenance and repair

II.3.2. Shadow

The two figures represent curves illustrating the effect of partial shading on the performance of photovoltaic systems. Figure A shows the relationship between electrical power and voltage under partial shade. The behavior is nonlinear and exhibits multiple peaks, reflecting the varying efficiency of solar cells due to some being shaded while others remain in optimal operation. These multiple peaks indicate the presence of multiple maximum power operating points (MPPs), making the maximum power point tracking (MPPT) process more complex and increasing the likelihood of the system reaching suboptimal power points. Figure B shows the current-voltage relationship for a solar cell under the same effect. The current starts constant at low voltage and gradually decreases as the voltage increases, with clear breaks in the curve due to the effect of the shade on the cells. Different current levels reveal the presence of multiple operating points, calling for the use of advanced technologies such as multi-point MPPT or bypass diodes to improve performance. Partial shading is an environmental factor that negatively impacts system efficiency, requiring effective engineering solutions to mitigate its impact.

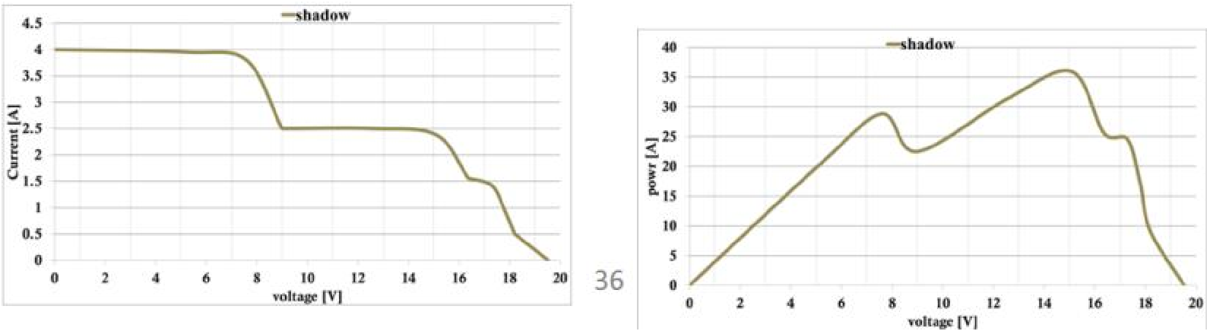

Figure II.12: shows the impact of partial shading on the PV panels. The I-V curves show large fluctuations and decreases compared to the healthy condition, which can significantly affect the system performance and power output.

II.3.3. Humidity

The graphs show how humidity affects a photovoltaic system's performance. Graph A plots power (amperes) versus voltage (volts). Power goes up as voltage increases, reaching a peak around 13.5 V, which is the best operating point. After this, power drops quickly, suggesting that humidity negatively impacts or some physical thing reduces performance at higher voltages. Graph B plots voltage versus current under the same conditions. Up to 7 V, the current stays steady at about 4 A, showing a stable conductivity area. Then, the current slowly goes down as voltage goes up, probably because humidity changes the electrical properties of the materials, such as raising resistance. The current drops sharply between 13 and 16 volts, which means the system is breaking down or reaching saturation. The drop keeps happening until the current hits zero at 20 volts, showing that there's no conductivity left because of moisture and high voltage together.

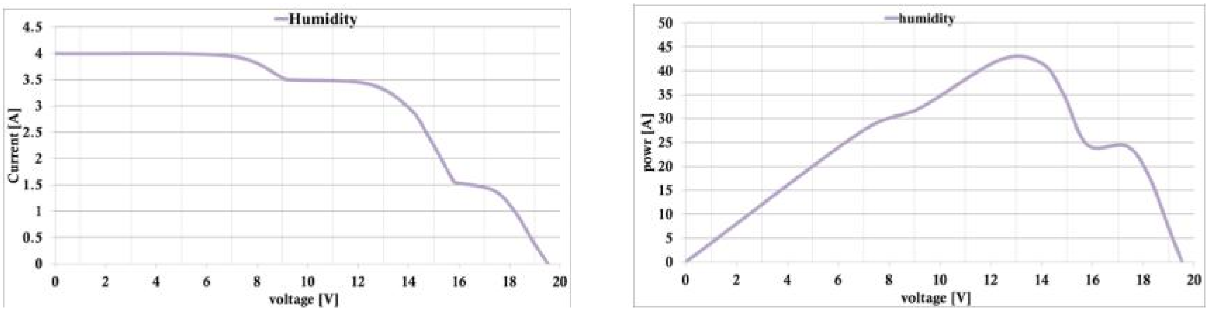

Figure II.13: shows the impact of the humidity intensity on the PV system. The I-V curves are irregular and show decreased efficiency, indicating the need for moisture protection measures

II.3.4. Short circuit

These two graphs show how a photovoltaic system acts when there's a short circuit. Graph A shows how voltage and power relate. Power goes up as voltage increases, peaking at about 11 V. This is the point where the system works best. After this, power drops fast, meaning there's a short circuit. A big current flows without a good load, so power is lost quickly. This unusual action suggests there are problems inside or the system is damaged. It's important to protect the system and check it regularly to avoid serious issues. Graph B shows how current and voltage relate in a solar cell. Current starts high (about 4.2 A) when voltage is zero. This is called the short-circuit current. As voltage goes up, current slowly goes down, almost reaching zero at about 13 V. This is the open-circuit voltage. The graph shows current dropping quickly before hitting zero. This spot is the maximum power point (MPP), which shows when the system is most effective under good lighting. This graph shows how a solar module usually works and why it's important to track the MPP to get the most sunlight.

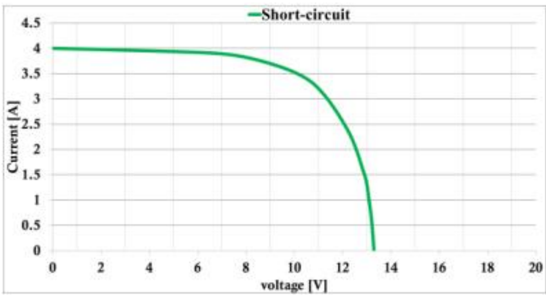

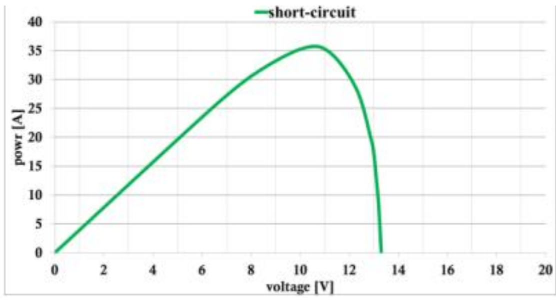

Figure II.14 : shows the impact of short circuit in PV system. The I-V curves exhibit a significant voltage drop which emphasizes the need for regular maintenance.

II.3.5. PV degradation

Figures A and B show how natural decay affects how well a solar power setup works.

Figure A has two curves that show how voltage and power relate to each other and how voltage and current relate. In Figure A, as voltage goes up, power also goes up little by little until it hits its highest point at about 13 V. After that, if the voltage keeps going up, the power starts to drop off slowly. This tells us that the system is getting less good over time because of natural decay from things like heat, ultraviolet light, and dampness. These things hurt how well the whole system works, but they don't make the curve change a lot all of a sudden, which proves that the decay is happening naturally from inside the system.

Figure B shows how current and voltage relate. The current begins high and stays almost the same until the voltage gets to about 11 V. Then, it slowly goes down until it hits zero when the circuit is open. This gradual drop shows that the solar cells are wearing out slowly because of heat expansion and weather conditions. Again, there are no sharp changes, so this is also natural decay, not sudden breaks. Watching these curves regularly is very important for figuring out how fast the system decays each year, putting in place methods like MPPT, and making better maintenance plans to keep the solar system working well over its life.

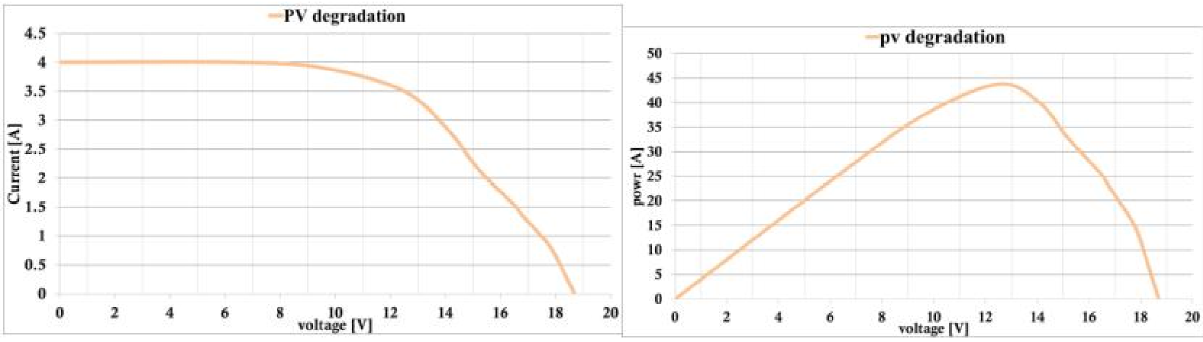

Figure II.15:shows the impact of degradation of PV panels with time. The I-V curves show a gradual decrease in performance, indicating the importance of timely repair and replacement of old deteriorating components.

II.4. .Conclusion

System modeling and the study of external influences are important for understanding and designing complicated systems. Modeling simplifies reality and helps predict how a system will act. Studying outside influences allows one to find the key things that impact how well it does. This method supports well-informed decisions and flexible strategies, leading to systems that are strong and can last.

Chapter III

Test and Application

III.1. Introduction

Health monitoring and fault detection in photovoltaic (PV) systems are essential for maximizing efficiency and lifespan. Deviations in current-voltage (I-V) curves indicate potential faults, requiring advanced diagnostic methods. This study presents an AI-enhanced approach combining optimization and classification for accurate fault analysis. A DC/DC buck-boost converter is implemented for real-time I-V data extraction. The proposed method improves reliability and reduces maintenance costs in PV power plants. This research contributes to smarter, more sustainable solar energy management.

III.2. Explantation of the applied part

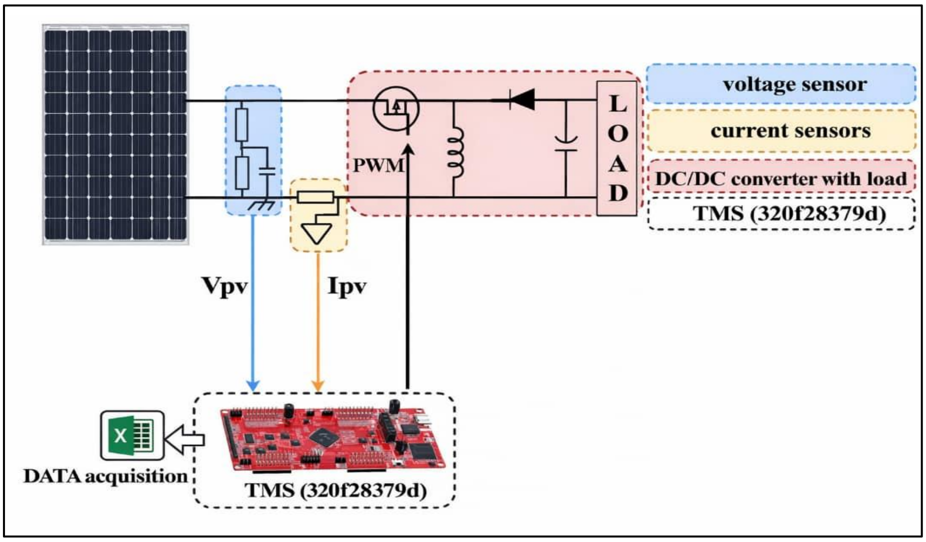

Figure III.1 : Proposed Circuit for Extracting Voltage-Current Characteristics Using a DC-DC Buck-Boost

III.2.1. Main Components in the Circuit

Voltage Sensor:

Measures the voltage (Vpv) coming from a power source such as solar panels or batteries.

Current Sensor:

Measures the current (Ipv) coming from the same source.

Buck-Boost DC/DC Converter:

Used to convert voltage and current to appropriate levels (stepping up or down) depending on the load settings.

Load:

Represents the device or circuit that consumes electrical power, such as a resistor or motor.

TMS Control Module (Reference Number: 320128379d):

power management and control system used to adjust the operation of the Buck-Boost converter, such as changing the duty cycle.

Data Acquisition Module:

Collects readings from sensors and stores them to analyze voltage and current characteristics -

III.2.2. Circuit Operation Steps

• Measuring Source Voltage and Current (Vpv and Ipv) Sensors measure voltage and current on the primary (source) side of the circuit. These readings are sent to a data acquisition unit for recording and analysis.

•Power Conversion via a Buck-Boost Converter

The converter operates in either Buck or Boost mode, depending on the load and control settings provided by the TMS.

Buck mode: The voltage is reduced if the source voltage is higher than the load voltage.

Boost mode: The voltage is increased if the load voltage is higher than the source voltage.

The conversion ratio is controlled by changing the duty ratio of the PWM signal received from the TMS.

•Connecting the Load

The load is connected to the secondary side of the converter.

The current flowing through the load is determined by the converter's characteristics and control settings.

•Data Collection and Analysis

The data acquisition unit records the voltage and current values on both sides (source and load). This data is used to plot the voltage-current curve (V-I curve).

III.2.3. Steps for Extracting Electrical Characteristics

•Power the circuit and stabilize the power supply (e.g., 24 VDC).

•Gradually change the load (e.g., using a variable resistor).

•Record the Vpv and Ipv values with each load change.

• Use the TMS module to adjust the converter's operation and maintain system stability.

•Plot the curve using the recorded data: Horizontal axis: Current (Ipv). Vertical axis: Voltage (Vpv).

III.2.4. Parallel Connection of Cells :

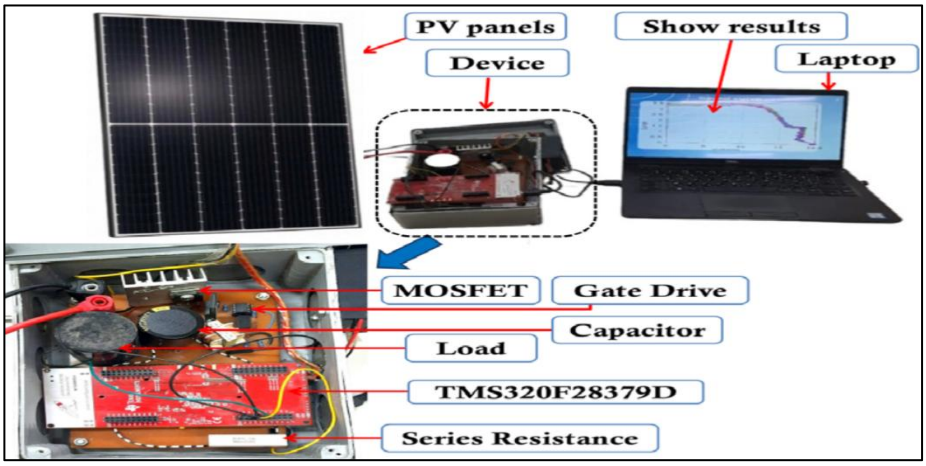

Figure III.2: Experimental Test Bench for Integrating the PV System and Buck-Boost Converter Controlled by the TMS320F28379D LaunchPad.

in components such as inductors, capacitors,and semiconductor switches. The Buck-Boost curve starts with the load increasing from zero, and at a duty cycle of around 0.5, the PV panel appears directly connected to the load. Beyond this, the Boost mode maximizes power output, covering all functional points and providing a more accurate VI curve compared to using only Boost or Buck converters.

(1) the role of every component in the system :

- **PV Panel :**

Converts solar energy into DC electrical power (voltage and current) that supplies the system under test.

- **MOSFET (Electronic Load) :**

It regulates the amount of current drawn from the PV panel, allowing the system to test different operating points of the panel

- **Gate Driver :**

Provides the required gate voltage and current to switch the MOSFET efficiently and safely.It isolates the low-power controller from the high-power stage.

- **TMS Controller:**

Processes measured data and executes control algorithms.
It generates PWM control signals to regulate the MOSFET and manage the system operation.

- **Voltage Sensor :**

Measures the output voltage of the PV panel.
This information is essential for monitoring, control, and system analysis.

- **Capacitor :**

Stores energy temporarily and smooths voltage fluctuations.
It reduces ripple and improves the stability of the DC output.

- **Series Resistance :**

Limits excessive current to protect system components.
It also helps stabilize the electronic load operation.

- **Communication Interface :**

Transfers measured data and control information between the controller and the laptop (e.g., USB, UART, or CAN).

- **Laptop :**

Used for programming the controller, receiving data, and displaying results such as I–V and P–V curves.

III.3. Applied results display

After using the previous device, several results were extracted under several variable conditions, including dust, shade, humidity, short circuit, and deterioration. The analytical results for all phenomena were presented. A curve was extracted. (I-V curve) and (P-V curve)

III.3.1. Dust

Figure A (I-V curve) and Figure B (P-V curve) clearly and gradually demonstrate the impact of dust accumulation on photovoltaic performance. In Figure A, we observe a significant decrease in the short-circuit current (Isc) as the dust level increases from level 1 (blue) to level 4 (red), while the open-circuit voltage (Voc) remains relatively constant, indicating that the losses are primarily due to the decrease in the amount of light transmitted to the cell surface.In Figure B, the curve shows a decline in the maximum power point (MPP) and a decrease in the output power with increasing dust accumulation, indicating a direct impact on the efficiency of the photovoltaic system. The maximum power decreases significantly, resulting in operational losses that can reach high percentages if neglected. This deterioration is associated with increased surface resistance caused by the dust layer, as well as reduced photon absorption efficiency, which distorts the performance curves. The analysis highlights the importance of regular maintenance and panel cleaning to maintain stable performance and ensure energy production in dusty environments.

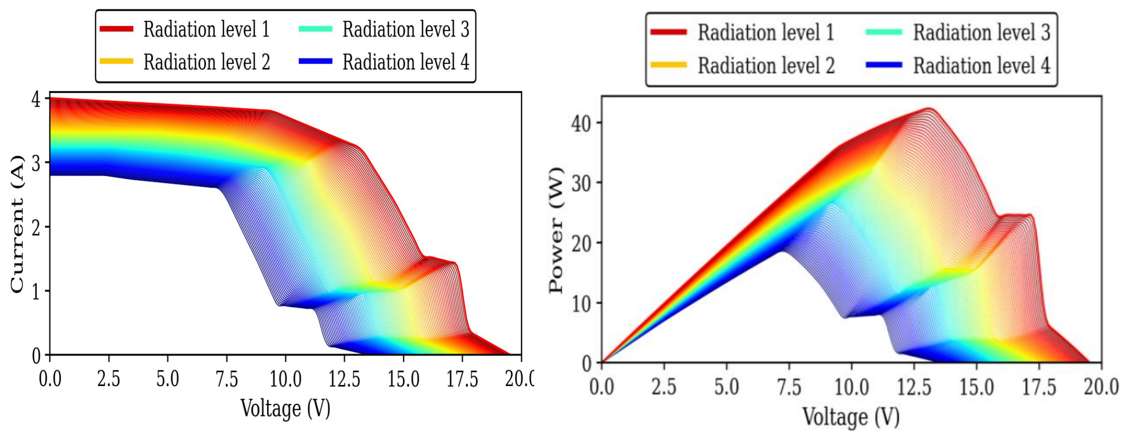

(A) (B)

Figure III.3: The effect of dust on solar panels . (I-V curve) and (P-V curve)

III.3.2. Shadow

In Figure (A), which represents the current-voltage (I-V) curve under shade, we observe that the current gradually decreases as solar radiation levels decrease from Level 1 to Level 4. This indicates that solar radiation intensity directly affects the amount of current generated in the solar cell. The maximum cell voltage also gradually decreases with decreasing radiation, indicating poor electrical performance under shaded conditions. Figure (B), which represents the power-voltage (P-V) curve under the same conditions, clearly shows a decrease in the maximum power point (MPP) with decreasing radiation levels. We observe that the highest power is generated at the first radiation level, while it decreases significantly at other levels, reflecting the direct relationship between solar radiation and power output. The shape of the curve also becomes flatter and more distorted at lower levels, making it difficult to track the maximum power point. These results demonstrate that the effect of shadowing has a significant impact on the performance of photovoltaic systems, leading to power losses and altering the electrical output characteristics of the cell. These findings are essential for designing shadow compensation systems or adopting techno logies such as MPPT to ensure optimal operation.

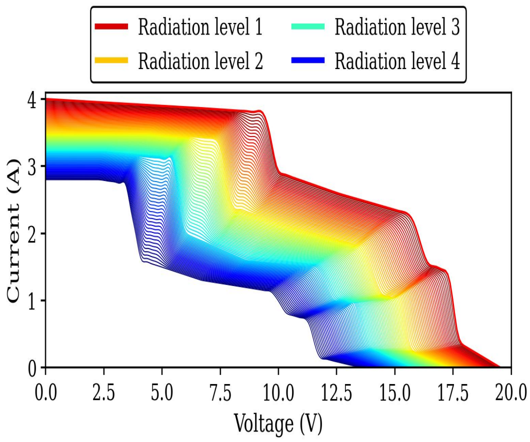

(A)

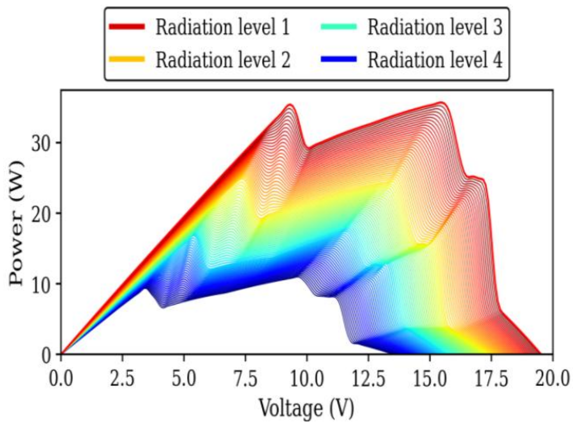

(B)

Figure III.4: The effect of shade on solar panels . (I-V curve) and (P-V curve)

III.3.3. Humidity

Figure (A) shows the current-voltage (I-V) curves under different humidity conditions at four solar radiation levels, while Figure (B) shows the power-voltage (P-V) curves for the same conditions. The results demonstrate that high humidity negatively affects solar cell performance. A clear decrease in current at the same voltage is observed as we move from Level 1 to Level 4, indicating a decrease in photovoltaic efficiency. In Figure (A), the blue curve (Level 1) shows the highest current, indicating the lowest humidity effect, while the red curve (Level 4) shows the lowest current. In Figure (B), the maximum power (Pmax) 47 Chapter III Analysis of Experimental Results gradually decreases with increasing humidity, indicating a clear effect on the output power. This decrease in power is associated with a decrease in both voltage and current at the maximum power point. We also note that the shape of the curve becomes less steep and more distorted at high humidity, reflecting the presence of additional losses in the system. These results demonstrate that humidity reduces the efficiency of solar cells due to water vapor absorption of light, reducing the effective radiation incident on the cell, and potentially causing changes in the cell's surface properties. Therefore, humidity control is recommended to improve the performance of photovoltaic systems, especially in regions with humid climates.

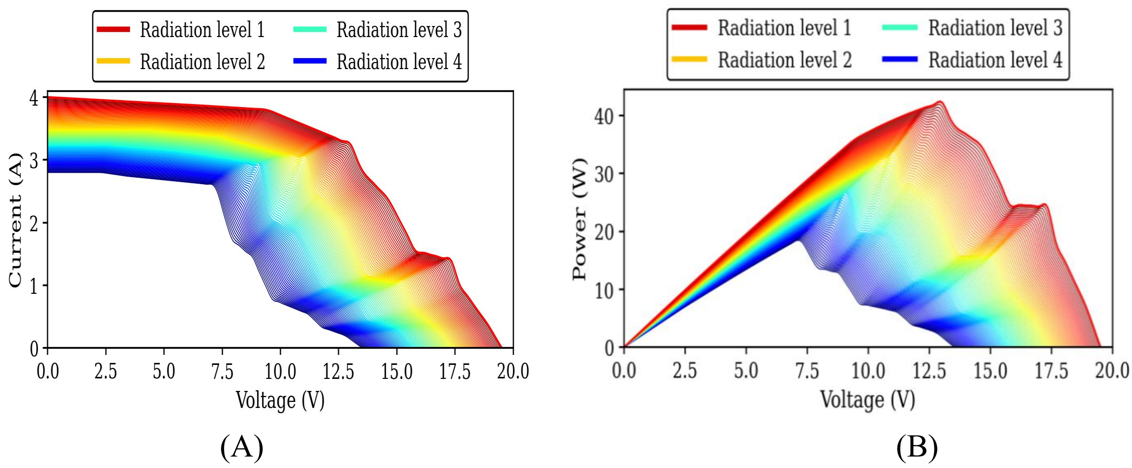

Figure III.5: The effect of humidity on solar panels . (I-V curve) and (P-V curve)

III.3.4. Short circuit

The electrical curves of a solar cell in a short circuit are an important diagnostic tool for understanding the performance of a photovoltaic system. Figure (A) shows the current voltage (I-V) curve under varying irradiance levels. The short-circuit current (Isc) increases directly with the intensity of light radiation, reaching its highest value at the maximum irradiance level (Level 4) and its lowest value at the minimum level (Level 1). The curve has a constant linear slope, reflecting the nature of the cell's internal resistance, with a clear intersection with the voltage axis at the theoretical open-circuit voltage.Figure (B) shows the power-voltage (P-V) curve, revealing a nonlinear relationship where the power reaches near zero values in this case. The curve exhibits an inverted hyperbolic shape with a weak peak representing the transition point between the two modes of cell operation. It is worth noting that the area under the curve is almost zero, indicating a near-total loss of useful electrical power.

These results confirm that short circuits are a practically undesirable situation, as the absence of an effective potential difference prevents the exploitation of the generated photovoltaic energy. They also highlight the importance of short circuit protection systems in practical solar system designs. These curves provide valuable data for energy engineers to understand the internal properties of cells and develop more efficient and safer systems.

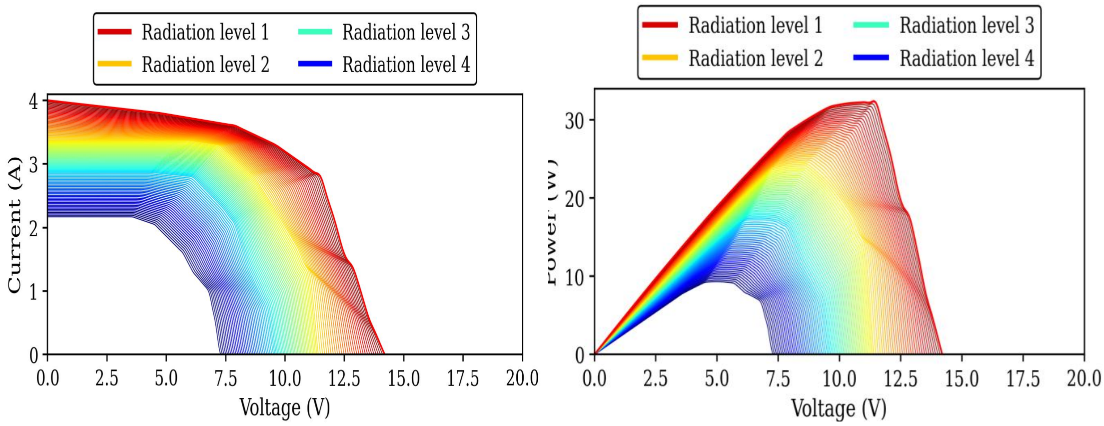

(a) (b)

Figure III.6: The effect of short circuit on solar panels (I-V curve) and (P-V curve)

III.3.5. Degradation

Figure A shows the relationship between current (A) and voltage (V) for four irradiance levels (Level 1 to Level 4) under photovoltaic cell degradation conditions. We observe that the current decreases with increasing voltage, a typical behavior for solar cells due to increased internal resistance. Higher irradiance levels (such as Level 1) exhibit higher current at lower voltages, reflecting higher energy conversion efficiency. Degradation is demonstrated by a decrease in current at the same voltage levels compared to ideal conditions, indicating a loss in performance due to factors such as corrosion or cracking. Figure B (P-V Curve) :Figure B shows the relationship between power (W) and voltage (V) for the same irradiance levels. We observe a peak power point (MPP) for each level, whose value decreases as the irradiance level decreases. Degradation is evident by a decrease in the maximum power and its shift toward lower voltages, indicating a loss in efficiency. The curve also shows a variation in the peak shape, becoming flatter with degradation, reflecting increased heat loss or junction resistance. The results confirm that degradation negatively impacts cell performance, as the peak current and power decrease as the curve characteristics change. These analyses are the basis for assessing cell life and improving their maintenance.

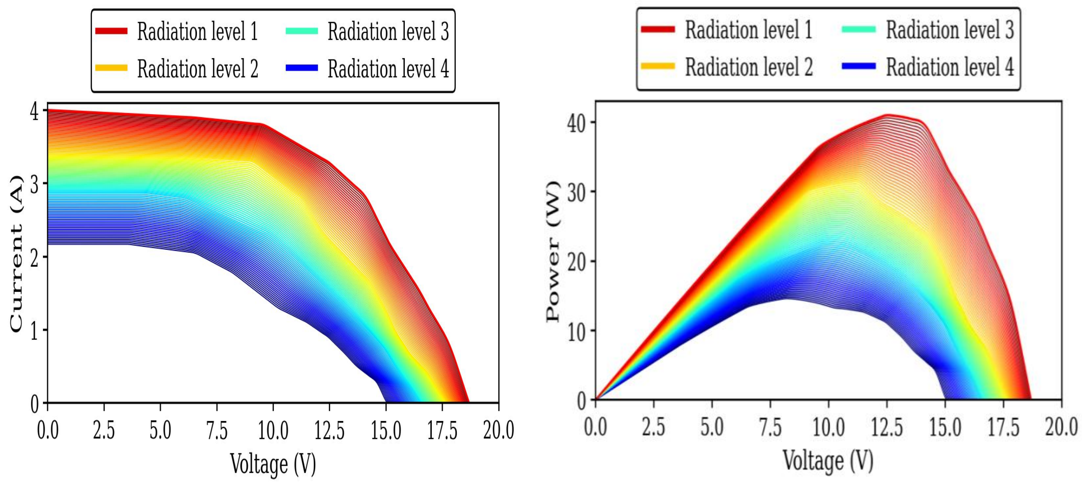

(A) **(B)**

Figure III.7: Effect of photovoltaic cell degradation . (I-V curve) and (P-V curve)

III.4 Conclusion:

This study highlights the importance of advanced diagnostic techniques in enhancing the performance and reliability of photovoltaic systems. By leveraging artificial intelligence alongside real-time I-V data extraction using a DC/DC buck-boost converter, the proposed approach enables accurate fault detection and efficient system optimization. Ultimately, this contributes to reducing maintenance costs and promoting smarter, more sustainable management of solar energy resourcesr.

Chapter IV

AI-Based Fault Diagnosis of Photovoltaic Systems Using I–V Curve Analysis

IV.1. Introduction :

Renewable energy is gaining traction due to growing energy needs, the environmental cost of unsustainable sources, and the finite nature of fossil fuels [86, 87]. Solar energy is a main renewable option due to its green nature, low running costs, and simple tech needs [88, 89].

Photovoltaic (PV) systems, which change sunlight into power, are quickly spreading globally as solar cell tech improves and panel costs go down [90, 91]. Yet, issues like partial shading and changing conditions can hurt their performance [92, 93].

Looking at I–V curves helps check PV system performance and spot problems [9]. Artificial intelligence (AI) methods, like enhanced artificial neural networks, ensemble learning, and combined deep learning models, have proven useful for real-time system checks and correct problem identification [94,95].

This paper puts forward an AI method to study I–V curves and find PV system faults. The aim is to improve performance, speed up response times, and keep systems working well in different settings.

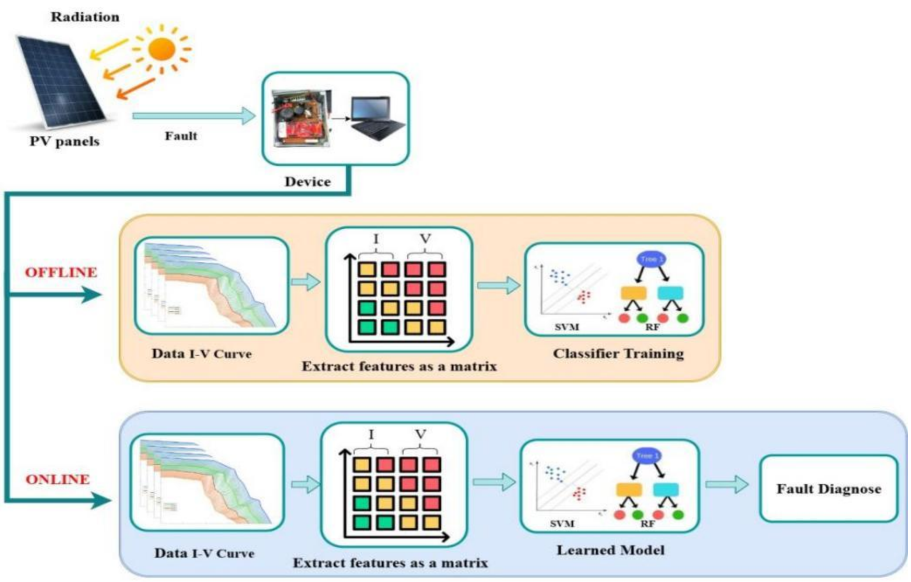

Figure IV. 1 : Block diagram of the proposed methodology for fault diagnosis

IV.2. Foundations of Machine Learning (ML)

Machine Learning (ML) is a subfield of artificial intelligence that focuses on developing computational methods that allow systems to automatically improve their performance on a task through experience. Unlike traditional programming, where explicit rules are coded for every scenario, ML systems learn patterns and relationships from data to make predictions, classifications, or decisions[102].

The foundation of ML combines mathematical modeling, statistical analysis, optimization theory, and computer science techniques to construct models that can generalize from observed data to unseen scenarios. This ability to generalize is central to ML and distinguishes it from memorization or simple rule-based systems[103].

Machine learning tasks are commonly formulated as constrained or unconstrained minimization problems. The learning process involves optimizing a loss function that quantifies the discrepancy between predicted and actual outputs. Regularization techniques are often incorporated to penalize overly complex models and improve generalization, particularly when dealing with noisy or limited datasets [104].

The theoretical foundations of machine learning provide the essential mathematical and algorithmic framework for constructing intelligent models capable of learning from data. These foundations enable machine learning methods to operate effectively in high-dimensional and nonlinear problem domains, making them well suited for advanced diagnostic and decision-support applications [105].

IV.3. Types of Machine Learning

IV.3.1. Supervised Learning Concept

Supervised Learning is a central paradigm in machine learning in which a model is trained using labeled data to learn the underlying relationship between input features and corresponding output labels. In this framework, the learning algorithm is “supervised” by the provided labels, meaning it receives direct feedback on its predictions during training. This enables the model to generalize from the observed examples and make accurate predictions for new, unseen data. [106]

The supervised learning paradigm provides a robust theoretical foundation for developing intelligent diagnostic systems. Its reliance on labeled data allows models to achieve high predictive accuracy and interpretability, making supervised learning particularly suitable for classification-based decision support and fault diagnosis tasks in complex engineering systems [107]

IV.3.2. Unsupervised Learning

Unsupervised Learning is a key paradigm in machine learning where the algorithm is trained on unlabeled data, meaning that the output labels yi are unknown. Instead of being guided by correct answers, the algorithm explores the structure and patterns within the input data xi to identify relationships, groupings, or underlying distributions[108].

In contrast to supervised learning, unsupervised learning focuses on discovering hidden patterns, clusters, or representations in the data, rather than predicting specific outputs.

Learning methods are widely used across various fields, including customer behavior analysis, image and text processing, fraud detection, and organizing large datasets. These methods are particularly useful when labeled data are unavailable or difficult to obtain, making them a powerful tool for exploratory data analysis and understanding the internal structures of complex systems[109].

Reinforcement Learning

Branch of machine learning that focuses on sequential decision-making through the interaction of a model, known as an agent, with its surrounding environment. In this type of learning, the agent is not provided with predefined correct outputs for each state. Instead, it learns through trial and error by receiving rewards or penalties based on the actions it takes. The agent's primary objective is to maximize the cumulative long-term reward, that is, to learn an optimal policy that achieves the best possible outcomes[110].

Reinforcement Learning (RL) is a fundamental paradigm of machine learning in which an agent learns to make decisions by interacting with an environment. Unlike supervised learning, RL does not rely on labeled input-output pairs; instead, the agent learns through trial and error by receiving feedback in the form of rewards or penalties. The objective of the agent is to learn a policy that maximizes the cumulative reward over time[111].

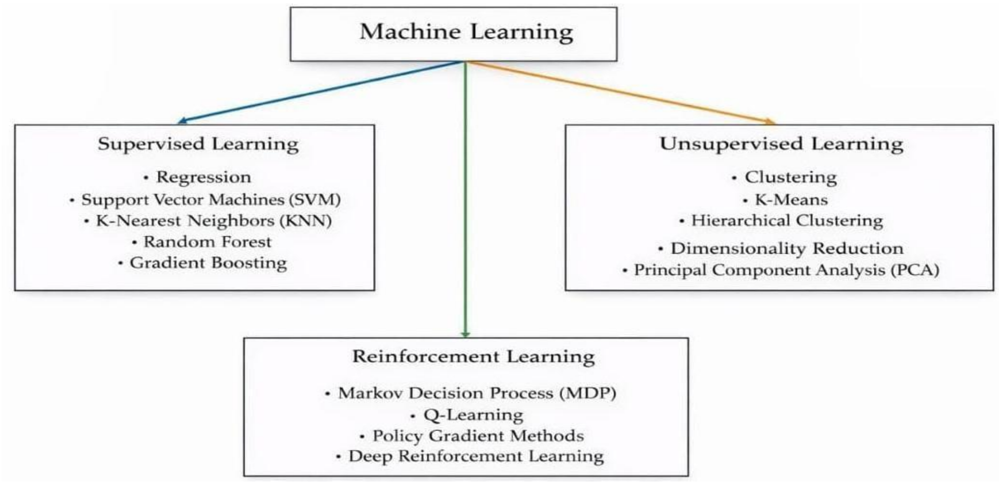

Figure IV.2 Taxonomy and Paradigms of Machine Learning Methods

IV.3.3. Deep Learning

Deep Learning (DL) is a subfield of machine learning that focuses on learning data representations through artificial neural networks (ANNs) with multiple layers. Unlike traditional machine learning models, which often rely on manually engineered features, deep learning models can automatically extract hierarchical features from raw data, enabling them to handle complex, high-dimensional data such as images, audio, and natural language [112].

IV.3.4. Ensemble Learning

Ensemble Learning is a machine learning approach that consists of combining multiple base learners to produce a final model that is more accurate and stable. This approach is based on the principle that aggregating several models helps reduce bias and variance errors, thereby improving the model's generalization ability [113].

This framework is built upon three main components:

(1) Base Learners:

These can be homogeneous models (e.g., multiple decision trees) or heterogeneous models (e.g., combining SVM, KNN, and decision trees).

(2) Diversity Mechanism:

Ensures variation among models through techniques such as bootstrap sampling, hyperparameter tuning, or using different algorithms.

(3) Aggregation Strategy:

Combines model outputs using methods such as majority voting for classification, averaging for regression, or a meta-learner in the case of stacking.

Ensemble Learning techniques are generally categorized into three main strategies:

Bagging: e.g., Random Forest, which reduces variance by training models on different data samples.

Boosting: e.g., XGBoost, where models are trained sequentially, each focusing on correcting the errors of previous ones [114].

IV.4. Study of Proposed Classification Algorithms

IV.4.1. Support Vector Machine (SVM)

(SVM) represent one of the advanced classification methods in machine learning and were developed based on Vapnik's research in the 1990s. This algorithm relies on a discriminant function to determine the optimal hyperplane that effectively separates different classes within a dataset. SVM is recognized for its high accuracy and robustness in classification, whether dealing with linear or nonlinear data, making it well-suited for data mining applications and complex analyses [115]. Figure IV.3 illustrates the general structure of the SVM algorithm, which works by identifying the optimal separating hyperplane, mathematically defined by the following equation:

$$f(x)=w^{\mathrm{T}}x+b \quad \text{for all } i \qquad \text{(IV.1)}$$

Where w is the weight vector, x is the input feature vector, and b is the bias. The objective is to maximize the margin $2\|w\|$ between the classes, subject to the constraints w is the weight vector, x is the input feature vector, and b is the bias. The objective is to maximize the margin $\frac{2}{\|w\|}$ between the classes, subject to the constraints:

$$w^{T}x_i + b) \geq 1 \qquad (IV.2)$$

y_i the effectiveness of Support Vector Machines (SVM) largely depends on the selection of the Kernel Function, which enables the transformation of the input space into a higher-dimensional feature space. This transformation allows the model to perform linear discrimination efficiently, even when dealing with complex or nonlinear data [116].

Kernel Trick can be represented as

$$K(xi,xj)=\phi(xi)^{T}\phi(xj) \qquad (IV.3)$$

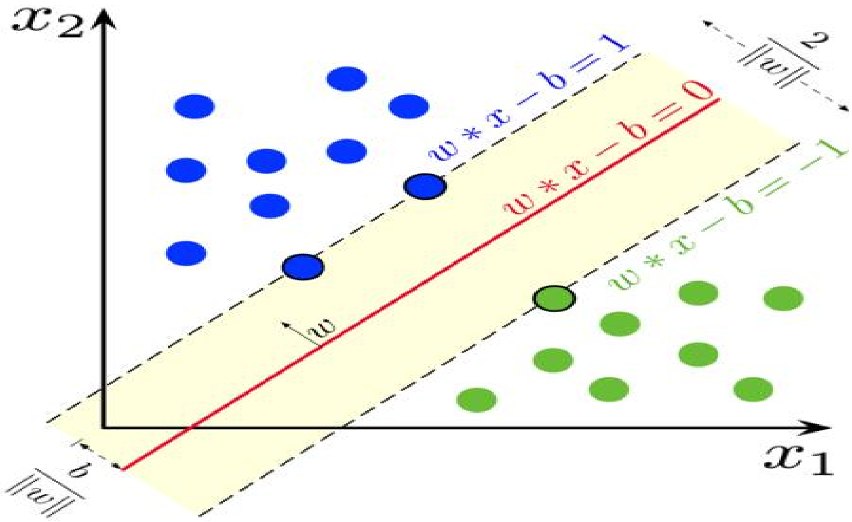

FigureIV.3 Enhanced Hyperplane Optimization in SVM for High-Dimensional Data Classification.

IV.4.2. k-Nearest Neighbors (k-NN)

The K-Nearest Neighbor (KNN) algorithm is considered one of the simplest learning algorithms, as it does not rely on a traditional training phase. Instead, it stores the training data and uses it directly during the classification process. Its mechanism is based on calculating the distance between a query point and the data points in the dataset, then selecting the closest k points. The class label assigned to the new point is determined by the class that appears most frequently among these nearest neighbors[117].

This can be mathematically expressed as:

$$y^\wedge = \text{argmax}c \sum_{j=1}^{k} (yj = \text{c}) \qquad (\text{IV}.4)$$

where I is an indicator function that equals 1 if the class label yj matches c and 0 otherwise. The distance between points is often measured using Euclidean distance:

$$d(x_i, x_j) = \sqrt{\sum_{k=1}^{n} (x_{ik} - x_{jk})^2} \qquad (\text{IV}.5)$$

This method enhances the classification process by extending the nearest neighbor concept, allowing the algorithm to leverage more information from multiple nearby points during the d

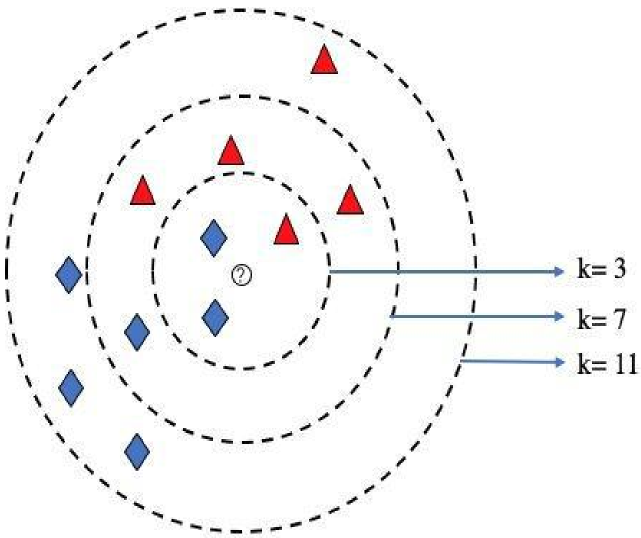

Figure IV .4 Principle of KNN algorithm with different k value

IV.4.3. Decision Trees (DT)

Decision Trees (DT) are a widely recognized classification algorithm known for their relatively simple structure. They excel at accurately analyzing substantial amounts of data within a short timeframe, making them particularly well-suited for efficient mass data processing [118]. The DT classifier is constructed using a combination of internal nodes and leaf nodes, where internal nodes represent decision thresholds based on feature values, and leaf nodes correspond to the predicted class labels as in Figure IV.5. The training process involves recursively identifying the best partition at each node to minimize uncertainty about the class labels, commonly assessed through metrics such as Entropy and Gini Impurity [119].

Entropy is calculated as:

$$H(S) = -\sum_{i=1}^{c} p_i \log_2 p_i \quad \text{(IV.6)}$$

Gini Index is defined as:

$$IG(S, A) = H(S) - \sum_{v \in A} \frac{|S_v|}{|S|} H(S_v) \quad \text{(IV.7)}$$

where p_i is the probability of class i in set S.

Information Gain is used to determine the best feature to split on:

$$\text{Gini}(S) = 1 - \sum_{i=1}^{c} (p_i)^2 \quad \text{(IV.8)}$$

This process continues until the dataset is fully analyzed, ensuring that each path through the tree leads to a definitive classification outcome.

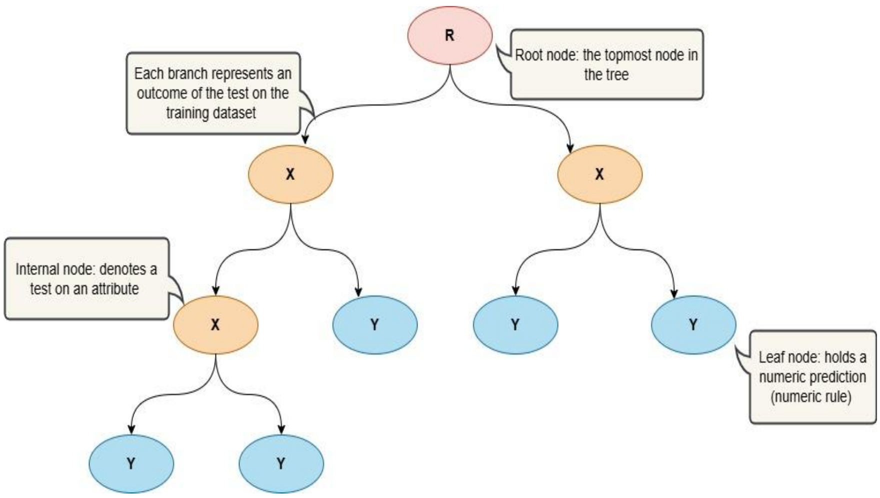

Figure IV.5 Decision tree structure

IV.4.4. XGBoost

The XGBoost algorithm, short for Extreme Gradient Boosting, is an advanced machine learning technique that relies on the principle of Gradient Boosting to build a strong model by combining a set of weak learners, typically small decision trees. It is designed to deliver faster and more efficient performance, with mechanisms to prevent overfitting and to handle large and complex datasets effectively.

XGBoost is widely used in competitive machine learning applications due to its high accuracy and flexibility. Its key features include support for missing value handling, parallel execution for faster training, and regularization techniques to reduce overfitting and improve generalization.

Used in competitive machine learning applications due to its high accuracy and flexibility. Its key features include support for missing value handling, parallel execution for faster training, and regularization techniques to reduce overfitting and improve generalization

IV.4.4.1 XGBoost Model (Ensemble of Trees)

In XGBoost, the model is expressed as a sum of weak learners (small decision trees):

$$\hat{y}_i = \sum_{t-1}^{T} f_t(x_i), \qquad f_t \in \mathcal{F} \tag{IV.9}$$

where:

- $\hat{y}_i$ is the model's prediction for sample i,
- T is the total number of trees,
- f_t represents a weak decision tree from the tree space $\mathcal{F}$
- x_i is the feature vector of sample.

IV.4.4.2 Classification Decision for Binary Classes

After computing i, the sigmoid function is used to convert it into the probability of belonging to class 1, followed by class assignment:

$$\left.\begin{matrix} \text{if } p_i \geq 0.5 \\ \text{if } p_i < 0.5 \\ 0 \end{matrix}\right\} = \ {}_{i}^{\text{class}} y, \frac{1}{\underline{i}-e+1} = (\hat{i}y)\sigma = \ {}_{i}p \tag{IV.10}$$

- Pi is the predicted probability of class 1,
- y^ i class is the final predicted class,
- σ (·) is the sigmoid function.

IV.4.4.3 XGBoost Multi-Class Classification Model

Explanation of the symbols in the equation:

$$\hat{y}_i = \arg \max_{k\in\{1,\dots,K\}} \frac{\exp\left(\sum_{m=1}^{M} f_{m,k}(x_i)\right)}{\sum_{j=1}^{K} \exp\left(\sum_{m=1}^{M} f_{m,j}(x_i)\right)} \tag{IV.11}$$

were

- x_i :The x_i-th sample (input instance).
- $\hat{y}_i$:The predicted class label for sample.
- K :The number of classes.
- k :Index of the current class.
- M :The number of trees (boosting rounds).
- m :Index of the tree.
- $f_{m,k}(x_i)$:The output of tree m for class k given input x_i.
- arg max: Selects the class with the highest probability.

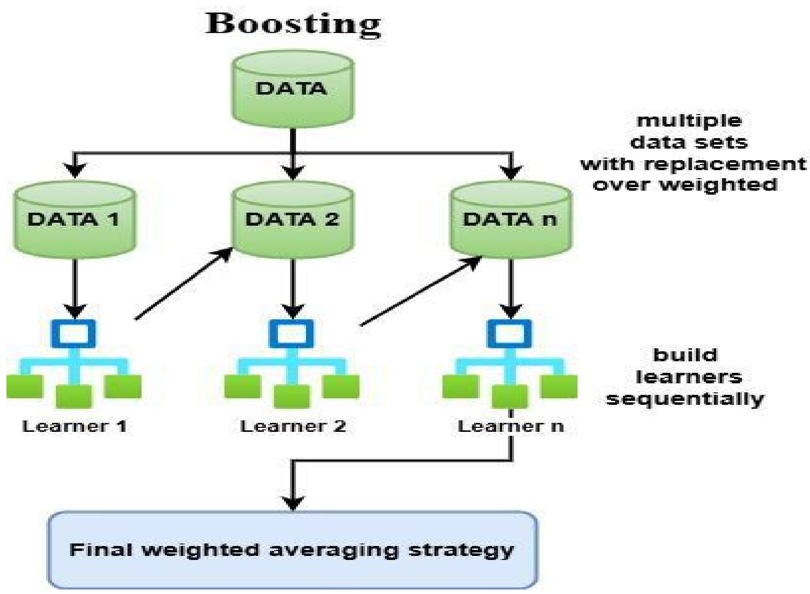

Figure IV.6 Structure of Boosting

IV.5. Performance evaluation metrics in classification

Are used to assess a model's ability to correctly classify samples into their respective categories. These metrics help compare different models, identify their strengths and weaknesses, and improve model performance before practical deployment.

IV.5.1 Accuracy

Represents the proportion of correctly classified samples out of the total samples:

$$\text{Accuracy}=\frac{TP}{TP+TN+FP+FN} \quad \text{(IV.12)}$$

Where:

TP (True Positives): Positive samples correctly predicted as positive

TN (True Negatives): Negative samples correctly predicted as negative

FP (False Positives): Negative samples incorrectly predicted as positive

FN (False Negatives): Positive samples incorrectly predicted as negative

Interpretation:

High accuracy → Most predictions (both positive and negative) are correct.

Low accuracy → Many predictions are wrong.

Suitable for balanced datasets, but may be misleading in the case of **imbalanced classes.**

IV.5.2 Confusion Matrix

The confusion matrix is a fundamental tool for summarizing classification performance, consisting of four elements in the case of binary classification:

	Predicted Positive	**Predicted Negative**
Actual Positive	True Positive (TP)	False Negative (FN)
Actual Negative	False Positive (FP)	True Negative (TN)

- **TP (True Positive):** Number of positive samples correctly classified.
- **TN (True Negative):** Number of negative samples correctly classified.
- **FP (False Positive):** Number of negative samples incorrectly classified as positive.
- **FN (False Negative):** Number of positive samples incorrectly classified as negative.

IV.5.3. Precision and Recall

Precision: The proportion of correctly predicted positive samples out of all samples classified as positive by the model:

$$\text{Precision} = \frac{TP}{TP+TF} \qquad \text{(IV.13)}$$

TP (True Positives): Correctly predicted positives

FP (False Positives): Incorrectly predicted positives

Interpretation:

High precision → Most of the predicted positives are correct.

Low precision → Many predicted positives are actually negative (false alarms).

Recall (Sensitivity): The proportion of positive samples correctly classified out of all actual positive samples:

$$\text{Recall} = \frac{\text{TP}}{\text{TP+FN}} \qquad \text{(IV.14)}$$

TP (True Positives): Correctly predicted positives

FN (False Negatives): Positives that the model missed

Interpretation:

High recall → The model catches most of the actual positives.

Low recall → The model misses many positives.

IV.5.4. F1-Score

The harmonic mean of precision and recall, particularly useful when dealing with **imbalanced classes:**

$$\text{F1}=2.\frac{\text{Precision}\cdot\text{Recal}}{\text{Precision}+\text{Recal}} \qquad \text{(IV.15)}$$

IV.5.5. ROC Curve and AUC

Plots True Positive Rate (TPR / Recall) vs False Positive Rate (FPR) at various thresholds.

Shows the model's performance across all possible thresholds, not just a fixed one.

Formulas:

$$TPR=\frac{TP}{TP+FN} \quad \text{(Recall)} \qquad (IV.16)$$

$$FPR=\frac{FP}{FP+TN} \qquad (IV.17)$$

TPR = fraction of actual positives correctly detected

FPR = fraction of actual negatives incorrectly classified as positive

AUC (Area Under the Curve): Represents the model's ability to discriminate between classes. The closer the AUC is to 1, the better the model performance.

Important Notes on Metric Selection

Balanced datasets: Accuracy is usually sufficient.

Imbalanced datasets: F1-Score or AUC is preferred.

High cost of false negatives (e.g., disease detection): Focus on **Recall.**

High cost of false positives (e.g., spam detection): Focus on **Precision.**

IV.6. Evaluation Metrics :

The effectiveness of AI classifiers in diagnosing panel conditions is evaluated using several key criteria. These criteria are essential in determining the overall performance of each model in accurate, real-time detection [100, 101].

$$\text{Accuracy} = \frac{\text{TP+TN}}{\text{N}} \qquad (IV.18)$$

$$\text{Precision} = \frac{\text{TP}}{\text{TP+FP}} \qquad (IV.19)$$

$$\text{Recall} = \frac{\text{TP}}{\text{TP+FN}} \qquad (IV.20)$$

$$\text{F1} - \text{Score} = 2 \text{ x } \frac{\text{Precision x Recall}}{\text{Precision+Recall}} \qquad (IV.21)$$

$$\text{Specificity} = \frac{\text{TN}}{\text{TN+FP}} \qquad (IV.22)$$

IV.7. Result and Discussion:

To evaluate the effectiveness of both the SVM and RF algorithms, based on I-V curve characteristics, designed to classify seven PV system states (Case 1 = Healthy, Case 2 = Dust, Case 3 = Shadow, Case 4 = Humidity, Case 5 = Open Circuit, Case 6 = Short Circuit, and Case 7 = PV Degradation), the test samples and the original dataset were obtained in a previous work [13]. Fig.3 shows the panel states obtained using the proposed monitoring device. The dataset consists of 658 samples, divided into 461 training samples and 197 test samples, and was analyzed using MATLAB. The following sections present the comparison results and evaluate the performance of the proposed models.

IV.7.1. Overall comparison of proposed models :

This Fig.IV.7 presents the confusion matrices for both the SVM model and the RF model. The matrices compare the true classes with the predicted classes across seven distinct cases, providing insight into the performance of both models.

SVM Confusion Matrix (A): The SVM model shows strong performance with 22 correct predictions for Case 1 and a perfect match for Case 6 (33 out of 33 correctly classified). However, there are some misclassifications in Case 2 (2 misclassified), Case 3 (2 misclassified), Case 4 (1 misclassified) and Case 7 (1 misclassified).

RF Confusion Matrix (B): The RF model performs similarly but shows improved results in Case 2 and Case 3, with 28 out of 28 correct predictions in Case 3. The RF model also has no misclassifications in Case 5 and Case 6, achieving 100% accuracy for these cases, while SVM had a few misclassifications in these areas.

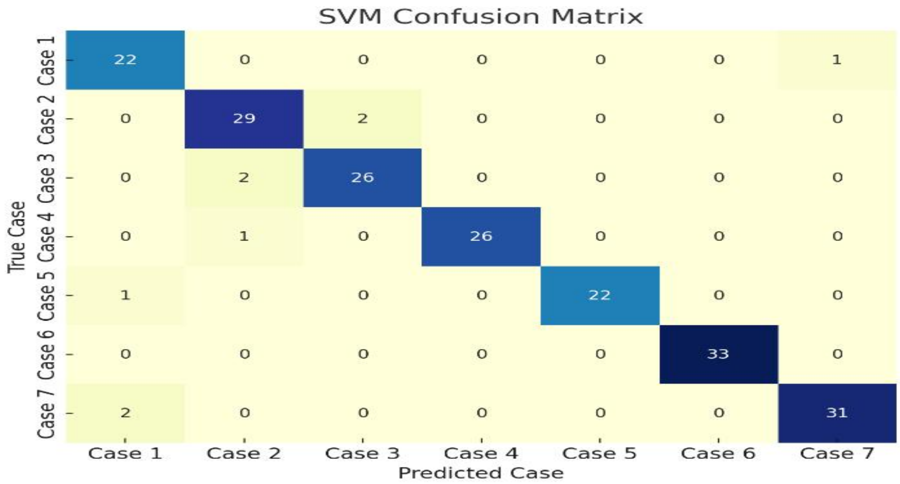

(A)

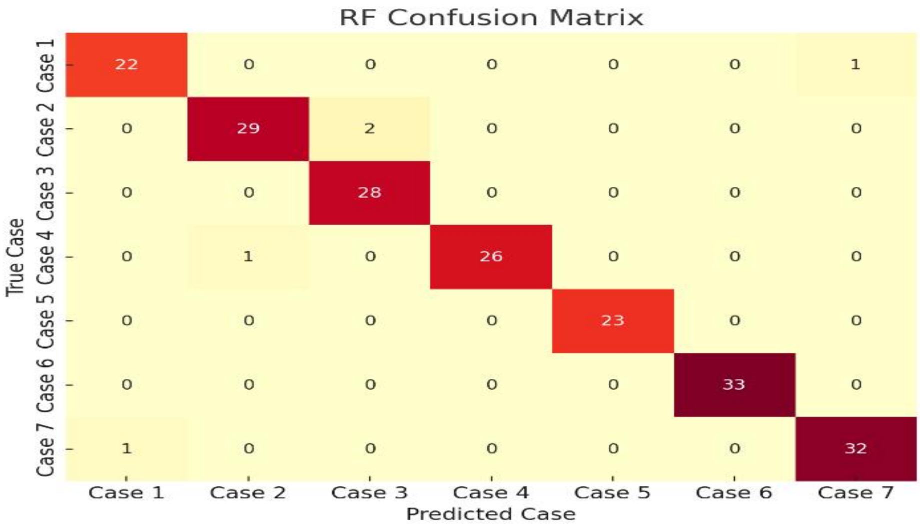

(B)

Figure IV.7. Confusion Matrix for model

The Table III and Fig.IV.8 presents the overall comparison between the SVM and RF models across several key metrics. RF consistently outperforms SVM in all aspects: it achieves 96.97% precision compared to 95.48% for SVM, and 97.50% recall, higher than 95.42% for SVM, indicating that RF is better at detecting true positive cases. The F1-Score for RF is 97.48%, surpassing SVM’s 95.41%, confirming its better balance between precision and recall. RF also shows better specificity (99.58%) and accuracy (97.47%) than SVM (99.24% and 95.45%, respectively). Overall, RF provides a more reliable and effective performance in fault detection for photovoltaic systems

IV.7.2. Performance evaluation of proposed models :

Table I shows the evaluation metrics for the SVM model across seven different test cases. The performance of the SVM model varies depending on the type of fault or condition affecting the PV system. Overall, the model performs well across all cases with precision, recall, and F1-Score values exceeding 90% in most cases.

Case 1 shows a precision of 88% and recall of 95.65%, achieving an F1-Score of 91.67%.

Case 4 demonstrates the best performance with 100% precision, a recall of 96.30%, and an F1-Score of 98.11%, showcasing the model's ability to handle more complex cases with high accuracy.

Case 6 achieves perfect scores across all metrics with 100% in precision, recall, F1-Score, and specificity.

The model performs slightly lower in Case 1 and Case 7, with precision and recall ranging between 88-96%, but specificity remains very high (above 98%).

These results indicate that the SVM model is effective at detecting faults across a wide range of conditions, with particularly strong performance in more ideal scenarios such as Case 6, where all metrics are at their maximum values.

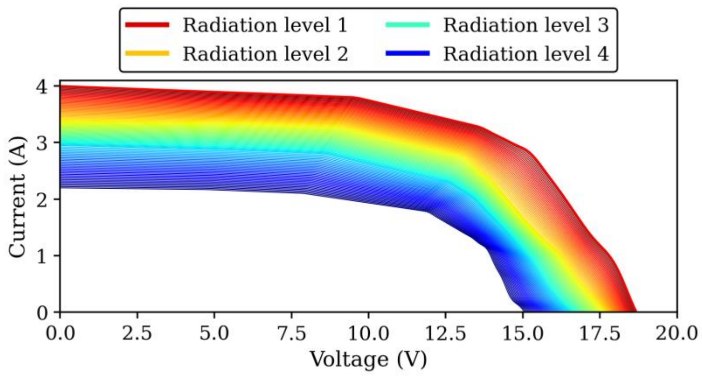

(A) Healthy

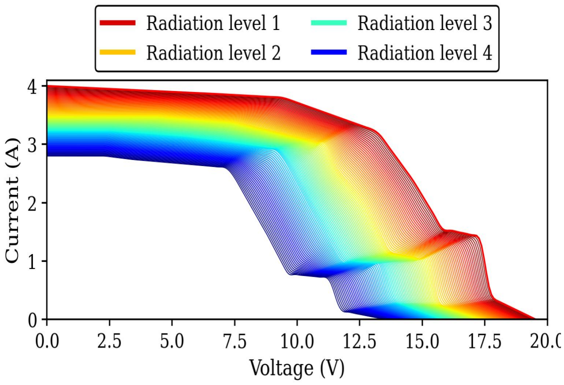

(B) Dust

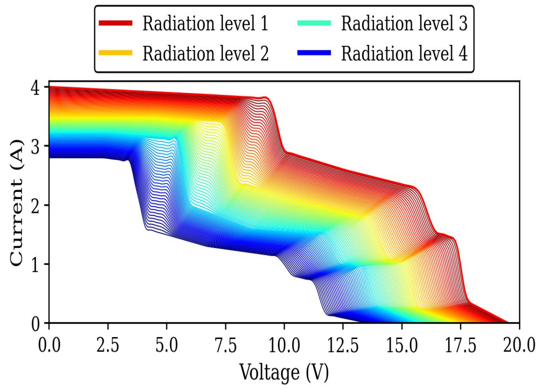

(C) Shadow

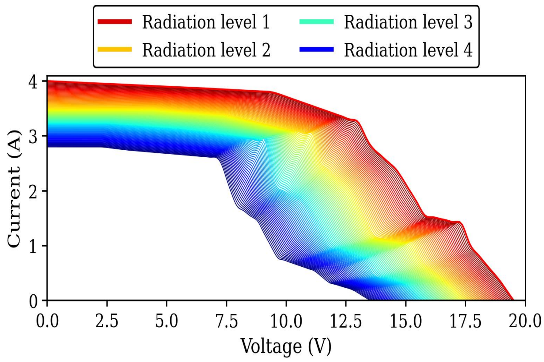

(D) Humidity

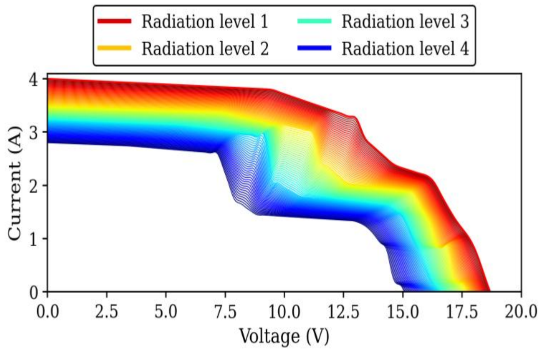

(E) Open Circuit

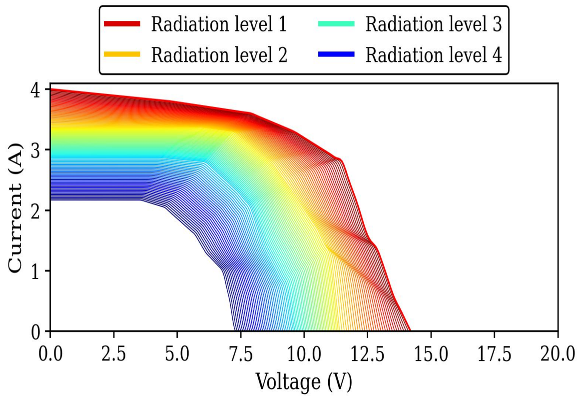

(F) Short Circuit

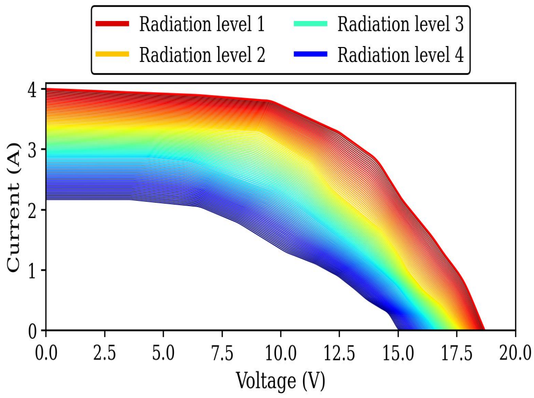

(G) PV Degradation

Table II displays the evaluation results for the Random Forest (RF) model across the same test cases. Like the SVM model, the RF model demonstrates robust performance across all cases, with precision, recall, F1-Score, and specificity consistently above 90%. However, the RF model performs slightly better than SVM in most cases, particularly in Case 1, Case 2, and Case 3.

Case 1 for RF shows precision and recall both at 95.65%, with an F1-Score of 95.65%, and specificity of 99.43%.

Case 3 performs with 100% recall, an F1-Score of 96.55%, and high specificity of 98.82%, indicating the RF model's strong ability to detect faults under a wide variety of conditions.

Case 6 also achieves perfect results with 100% across all metrics, similar to the SVM model.

In Case 7, the RF model achieves 96.97% for both precision and recall, with an F1-Score of 96.97% and specificity of 99.39%, showing solid performance even in the more challenging cases.

Table I SVM performance for different panel cases

Types of cases	**SVM evaluation metrics (%)**			
	Precision	Recall	F1-Score	Specificity
Case 1	88.00	95.65	91.67	98.29
Case 2	90.62	93.55	92.06	98.20
Case 3	92.86	92.86	92.86	98.82
Case 4	100	96.30	98.11	100.
Case 5	100	95.65	97.78	100
Case 6	100	100	100	100
Case 7	96.88	93.94	95.38	99.39

Table II RF performance for different panel cases

Types of cases	RF evaluation metrics (%)			
	Precision	Recall	F1-Score	Specificity
Case 1	95.65	95.65	95.65	99.43
Case 2	96.67	93.55	95.08	99.40
Case 3	93.33	100.0	96.55	98.82
Case 4	100	96.30	98.11	100
Case 5	100	100	100	100
Case 6	100	100	100	100
Case 7	96.97	96.97	96.97	99.39

Table III Overall comparison for model

Overall	SVM (%)	RF (%)
Precision	95.48	96.97
Recall	95.42	97.50
F1-Score	95.41	97.48
Specificity	99.24	99.58
Accuracy	95.45	97.47

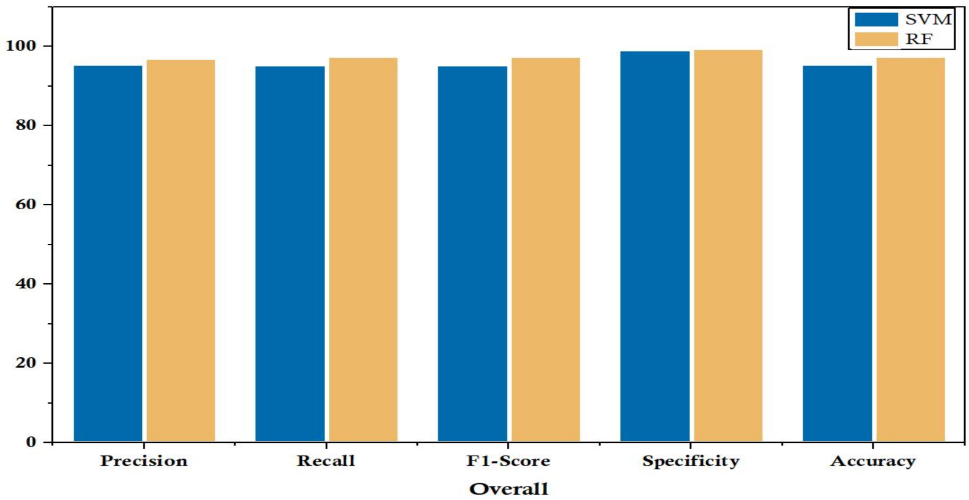

Figure.IV.8. overall comparison for mode

IV.8. Conclusion

This paper introduces a method for finding faults in PV systems. It uses real-time I-V curve study with artificial intelligence (AI). A DC/DC buck-boost converter gathers I-V data for correct fault finding. Random Forest (RF) and Support Vector Machine (SVM) models use AI to sort PV system faults. RF did better than SVM in key areas. RF got 96.97% precision, 97.50% recall, a 97.48% F1-score, 99.58% specificity, and 97.47% accuracy. SVM had 95.48%, 95.42%, 95.41%, 99.24%, and 95.45%, respectively. The findings suggest RF is an accurate, reliable, and efficient way to find faults and watch PV systems in real-time. This method, which joins machine learning and I-V curve study, may make solar energy systems easier to maintain and run. Future studies will add to the data set and test the method on bigger setups. This will check how well it works in real situations.

General Conclusion

This study explored ways to better find errors in solar panel systems by mixing electrical measurements and computer intelligence. It stressed how vital it is to get how solar panels change sunlight into power and act under changing conditions. This base is needed for making systems that are dependable in design and observation.

It was shown that correct models and studies of solar systems are key to judging how well they work. They assist in finding the impact of things like temperature, load, and setup. These things give good knowledge on how systems act. They back the making of strong ways to spot and fix the problems.

A main point of this study is using current and voltage plots done live with computer intelligence to spot errors. By adding a DC/DC converter to get live data with machine learning, a strong way to find errors got made. The data showed that ways using AI can correctly find errors and make system checks better. A model called Random Forest worked better than Support Vector Machine in being correct and exact.

In general, the plan given helps make solar systems more dependable, efficient, and easier to keep up. By finding errors early and backing good choices on fixes, this way helps cut running costs and back keeping solar power sources healthy. Work later will add more data, test the way given on bigger solar setups, and see how it does in real use. This will make it more helpful in present solar power system.

Reference

References

[1] T. Li, A. Li, and Y. Song, "Development and utilization of renewable energy based on carbon emission reduction—evaluation of multiple MCDM methods," Sustainability, vol. 13, no. 17, p. 9822, 2021.

[2] [M. K. G. Deshmukh, M. Sameeroddin, D. Abdul, and M. A. Sattar, "Renewable energy in the 21st century: A review," Materials Today: Proceedings, vol. 80, pp. 1756-1759, 2023.

[3] S. C. Aykut and A. Dahan, Gouverner le climat?. Vingt ans de négociations internationales. Sciences Po (Les Presses de), 2014.

[4] N. Tekbıyık Ersoy, "Technology Based Renewable Energy Policy Analysis," in Energy Efficiency and Renewable Energy Policies: Springer, 2024, pp. 99-102.

[5] M. Taylor, "Renewable Power Generation Cost Trends to 2022-Michael Taylor," 2023.

[6] Y. P. Siwakoti, F. Z. Peng, F. Blaabjerg, P. C. Loh, and G. E. Town, "Impedance-source networks for electric power conversion part I: A topological review," IEEE Transactions on power electronics, vol. 30, no. 2, pp. 699-716, 2014.

[7] J. Yuan, F. Blaabjerg, Y. Yang, A. Sangwongwanich, and Y. Shen, "An overview of photovoltaic microinverters: Topology, efficiency, and reliability," in 2019 IEEE 13th International Conference on Compatibility, Power Electronics and Power Engineering (CPE-POWERENG), 2019: IEEE, pp. 1-6.

[8] Y. Liu, H. Abu-Rub, B. Ge, F. Blaabjerg, O. Ellabban, and P. C. Loh, "Applications in Photovoltaic Power Systems," 2016.

[9] R. Panigrahi, S. K. Mishra, S. C. Srivastava, A. K. Srivastava, and N. N. Schulz, "Grid integration of small-scale photovoltaic systems in secondary distribution network—A review," IEEE Transactions on Industry Applications, vol. 56, no. 3, pp. 3178-3195, 2020.

[10] Z. Tang, Y. Yang, and F. Blaabjerg, "Power electronics: The enabling technology for renewable energy integration," CSEE Journal of Power and Energy Systems, vol. 8, no. 1, pp. 39-52, 2021.

[11] M. Islam, S. Mekhilef, and M. Hasan, "Single phase transformerless inverter topologies for grid-tied photovoltaic system: A review," Renewable and sustainable energy reviews, vol. 45, pp. 69-86, 2015.

[12] D. Meneses, F. Blaabjerg, O. Garcia, and J. A. Cobos, "Review and comparison of step-up transformerless topologies for photovoltaic AC-module application," IEEE Transactions on Power Electronics, vol. 28, no. 6, pp. 2649-2663, 2012.

[13] M. T. Outeiro, R. Visintini, and G. Buja, "Considerations in designing power supplies for particle accelerators," in IECON 2013-39th Annual Conference of the IEEE Industrial Electronics Society, 2013: IEEE, pp. 7076-7081.

[14] M. T. Outeiro, G. Buja, and A. Carvalho, "Resonant converters for electric equipment power supply," in IECON 2014-40th Annual Conference of the IEEE Industrial Electronics Society, 2014: IEEE, pp. 5065-5071.

[15] A. Richelli, M. Salem, and L. Colalongo, "A review of fully integrated and embedded power converters for IoT," Energies, vol. 14, no. 17, p. 5419, 2021.

[16] M. Monsalve-Rueda, J. E. Candelo-Becerra, and F. E. Hoyos, "Dynamic behavior of a sliding-mode control based on a washout filter with constant impedance and nonlinear constant power loads," Applied Sciences, vol. 9, no. 21, p. 4548, 2019.

[17] A. I. M. Ali, M. A. Sayed, and T. Takeshita, "Isolated single-phase single-stage DC-AC cascaded transformer-based multilevel inverter for stand-alone and grid-tied applications," International Journal of Electrical Power & Energy Systems, vol. 125, p. 106534, 2021.

[18] A. Nabae, I. Takahashi, and H. Akagi, "A new neutral-point-clamped PWM inverter," IEEE Transactions on industry applications, no. 5, pp. 518-523, 1981.

[19] . Fouad, M. M., Shehata, L. A., & Morgan, E. I. 2017. An integrated review of factors influencing the performance of photovoltaic panels. Renewable and Sustainable Energy Reviews, 80, 1499–1511. https://doi.org/10.1016/j.rser.2017.05.141

[20] S. Sumathi, L. Ashok Kumar, and P. Surekha, "RETRACTED CHAPTER: Wind Energy Conversion Systems," in RETRACTED BOOK: Solar PV and Wind Energy Conversion Systems: Springer, 2015, pp. 247-307.

[21] "Energías renovables," Solar Innova. Accessed: Oct. 24, 2021. [Online]. Available: http://solarinnova.com/

[22] "La boîte de jonction solaire photovoltaïque - Connaissances - DS New Energy," DSN Solar. Accessed: Oct. 23, 2021. [Online]. Available: https://www.dsnsolar.com/info/the- solar-pv-junctionbox-54220374.htm

[23] "Quelle est l'importance du cadre d'un module solaire?," aleo solar - France. Accessed: Oct. 23, 2021. Online. Available: https://www.aleo-solar.fr/importance-cadre-panneau-solaire/

[24] 1. Vechiu, "Modélisation et analyse de l'intégration des énergies renouvelables dans un réseau autonome," Université du Havre, 2005.

[25] 18. Viitanen, J. 2015. Energy-efficient lighting systems in buildings with integrated photovoltaic cells. Renewable and Sustainable Energy Reviews. Retrieved from https://aaltodoc.aalto.fi/handle/123456789/15265

[26] A. A. A. Radwan and Y. A.-R. I. Mohamed, "Power synchronization control for grid- connected current-source inverter-based photovoltaic systems," IEEE Transactions on Energy Conversion, vol. 31, no. 3, pp. 1023-1036, 2016.

[27] A. Omazic et al., "Relation between degradation of polymeric components in crystalline silicon PV module and climatic conditions: A literature review," Solar Energy Materials and Solar Cells, vol. 192, pp. 123–133, Apr. 2019, doi: 10.1016/j.solmat.2018.12.027.

[28] A. Samui and S. R. Samantaray, "New active islanding detection scheme for constant power and constant current controlled inverter-based distributed generation," IET Generation, Transmission & Distribution, vol. 7, no. 7, pp. 779-789, 2013.

[29] Bani, M. J. B., Al-Wali, A. K., Al-Kan, K., & Al-Asadi, K. 2018. Effect of Solar Irradiance on Photovoltaic Cell. International Journal of Advanced Engineering Research, 3- 3-, 47–51.

[30] Bright, J. M., Babacan, O., Kleissl, J., Taylor, P. G., & Crook, R. 2017. A synthetic, spatially decorrelating solar irradiance generator and its application to a low voltage network model with high PV penetration. Solar Energy, 147, 83–98. https://doi.org/10.1016/j.solener.2017.03.018

[31] C. Peike, I. Hädrich, K.-A. Weiß, and I. Dürr, "Overview of PV module," [Incomplete source: journal name, volume, year, pages needed].

[32] Chanchangi, Y. N., Ghosh, A., Sundaram, S., & Mallick, T. K. 2020. Dust and photovoltaic performance in Nigeria: A review. Renewable and Sustainable Energy Reviews, 121, 109704. https://doi.org/10.1016/j.rser.2020.109704

[33] Chegaar, M., Hamzaoui, A., Namoda, A., Bechouche, B., Allery, M., & Heraghty, A. 2013. Effect of Illumination Intensity on Solar Cell Parameters. Energy Procedia, 36, 722– 729. https://doi.org/10.1016/j.egypro.2013.07.084

[34] Dewi, T., Risma, P., & Oktarina, Y. 2019. A review of factors affecting the efficiency and output of a PV system applied in tropical climate. IOP Conference Series: Earth and Environmental Science, 258, 012039. https://doi.org/10.1088/1755-1315/258/1/012039

[35] E. Parnham, A. Whitehead, S. Pain, and B. Brennan, "Comparison of Accelerated UV Test Methods with Florida Exposure for Photovoltaic Backsheet Materials," in Proc. 33rd Eur. Photovoltaic Solar Energy Conf.

and Exhibition, 2017, pp. 1345–1348, doi: 10.4229/EUPVSEC20172017-5BO.5.5.

[36] International Energy Agency. 2010. Technology Roadmap: Solar Photovoltaic Energy. https://doi.org/10.1787/9789264088047-en

[37] International Renewable Energy Agency. 2021. Solar. Retrieved November 15, 2021, from https://www.irena.org/solar

[38] Islam, M. N., Rahman, M. Z., & Momenuzzaman, S. M. 2014. Different Parameters of Mono-crystalline Photovoltaic Solar Cell: Effect of Irradiance. In 3rd International Conference on the Developments in Renewable Energy Technology ICDRET pp. 1–6. https://doi.org/10.1109/ICDRET.2014.6861716

[39] J. M. E. Huerta, J. Castello, J. R. Fischer, and R. García-Gil, "A synchronous reference frame robust predictive current control for three-phase grid-connected inverters," IEEE Transactions on Industrial Electronics, vol. 57, no. 3, pp. 954 -962, 2009.

[40] J. Miret, A. Camacho, M. Castilla, L. G. de Vicuña, and J. Matas, "Control scheme with voltage support capability for distributed generation inverters under voltage sags," IEEE Transactions on Power Electronics, vol. 28, no. 11, pp. 5252-5262, 2013.

[41] J. Miret, M. Castilla, J. Matas, J. M. Guerrero, and J. C. Vasquez, "Selective harmonic-compensation control for single-phase active power filter with high harmonic rejection," IEEE transactions on industrial electronics, vol. 56, no. 8, pp. 3117-3127, 2009.

[42] J. S. Lim, C. Park, J. Han, and Y. I. Lee, "Robust tracking control of a three-phase DC–AC inverter for UPS applications," IEEE Transactions on Industrial Electronics, vol. 61, no. 8, pp. 4142-4151, 2013.

[43] Kazem, H. A., Chaichan, M. T., Al-Waeli, A. H. A., & Sopian, K. 2020. A review of dust accumulation and cleaning methods for solar photovoltaic systems. Journal of Cleaner Production, 276, 123187. https://doi.org/10.1016/j.jclepro.2020.123187

[44] L. Guo, J. Y. Hung, and R. Nelms, "Design and implementation of a digital PID controller for a buck converter," in IECEC-36 th Intersociety Energy Conversion Engineering Conference, 200 1, pp. 187-192.

[45] Liu, L. 2009. Comment on "Recent advances in radiation thermodynamics, photon effective temperature and photon entropy constant". Science in China Series E: Technological Sciences, 52(6), 1809–1810. https://doi.org/10.1007/s11431-009-0086-4

[46] M. Beza and M. Bongiorno, "Improved discrete current controller for grid-connected voltage source converters in distorted grids," in 2012 IEEE Energy Conversion Congress and Exposition (ECCE), 2012: IEEE, pp. 77-84.

[47] M. Ebadi, M. Joorabian, and J. S. Moghani, "Voltage look-up table method to control multilevel cascaded transformerless inverters with unequal DC rail voltages," IET power electronics, vol. 7, no. 9, pp. 2300-2309, 2014.

[48] M. Kandil, M. El-Saadawi, A. Hassan, and K. Abo-Al-Ez, "A proposed reactive power controller for DG grid connected systems," in 2010 IEEE International Energy Conference, 2010: IEEE, pp. 446-451.

[49] Mohanty, P., Muneer, T., Gajoo, E. J., & Kotak, Y. 2016. Fundamentals of Solar Radiation and Components of PV Systems. In P. Mohanty, T. Muneer, & M. Kohle Eds., Solar Photovoltaic System Applications: A Guidebook for Off-grid Electrification pp. 7–47. Springer, Cham. https://doi.org/10.1007/978-3-319-14663-8_2

[50] Mondol, J. D., Yohanis, Y. G., & Norton, B. 2007. Effect of array tilt and orientation on the performance of a grid-connected photovoltaic system. Renewable Energy, 32-1-, 118–140. https://doi.org/10.1016/j.renene.2006.05.006

[51] Prema, V., & Uma Rao, K. 2015. Development of statistical time series models for solar energy forecasting. Renewable Energy, 83, 100–109. https://doi.org/10.1016/j.renene.2015.03.038

[52] R. Chilipi, N. Al Sayari, K. Al Hosani, and A. R. Beig, "Control scheme for grid-tied distributed generation inverter under unbalanced and distorted utility conditions with power quality ancillary services," IET Renewable Power Generation, vol. 10, no. 2, pp. 140-149, 2016.

[53] Radziemska, E. 2003. The Thermal Performance of Silicon and Gallium Arsenide- Based Solar Cells and Modules: A Review. Renewable and Sustainable Energy Reviews, 29, 407–424

[54] Renewable Energy: Sustainable Energy Concepts for the Future. 2009. Choice Reviews Online, 46-05-, 46-2689. https://doi.org/10.5860/choice.46-2689

[55] S. Abouda, "Contribution à la commande des systèmes photovoltaiques: application aux syst èmes de pompages," Reims, 2015.

[56] S. Goya, Y. Nakano, N. Yamashita, S. Morita, and Y. Yonekura, "Development of amorphous sil icon/microcrystalline silicon tandem solar cells, in 3rd World Conference onPhotovoltaic Ener gy Conversion, 2003. Proceedings of, 2003, vol. 2: IEEE, pp. 1570-1573.

[57] S. Tahir, J. Wang, G. S. Kaloi, and M. H. Baloch, "Robust digital deadbeat control design technique for 3 phase VSI with disturbance observer," IEICE Electronics Express, vol. 14, no. 13, pp. 20170351-20170351, 2017.

[58] Salim, M. S., Najm, G. M., & Saleh, S. M. 2013. Experimental Evaluation of Solar Irradiance Impact on PV Energy Output. Energy Science and Technology, 6-2-, 36–40. https://doi.org/10.3968/j.est.1923847920130602.2671

[59] Santbergen, R., Muthukumar, V. A., Valckenborg, R. M. E., van de Wall, W. J. A., Smets, A. H. M., & Zeman, M. 2017. Calculation of irradiance distribution on PV modules by combining sky and sensitivity maps. Solar Energy, 150, 49–54. https://doi.org/10.1016/j.solener.2017.04.036

[60] Seeger, K. 2013. Semiconductor Physics. Springer Science & Business Media: Berlin/Heidelberg, Germany.

[61] Shah, A. S. B. M., Yokoyama, H., & Kakimoto, N. 2015. High-resolution solar radiation prediction model based on gridded data analysis for an efficient photovoltaic system. IEEE Transactions on Sustainable Energy, 6(2), 474–481. https://doi.org/10.1109/TSTE.2014.2383398

[62] Sharma, D., Mehra, R., & Raj, B. 2021. Comparative Analysis of Photovoltaic Techniques for Designing High-Efficiency Solar Cells. Superlattices and Microstructures, 153, 106861.

[63] Smets, A. H. M., Jäger, K., Isabella, O., van Swaaij, R. A., & Zeman, M. 2016. Solar Cell Parameters and the Equivalent Circuit. Solar Energy: Photovoltaics Systems Technology Conversations, 113–121.

[64] Smith, R. B., Hwang, A. A.-C., Betts, T., & Hillgren, E. 2018. Introduction to Semiconductor Processing: Fabrication and Characterization of Silicon p-n Junction Solar Cells. American Journal of Physics, 86, 740–746.

[65] Song, Z., Liu, J., & Yang, H. 2021. Air pollution and its effects on solar photovoltaic power generation: A comprehensive review. Applied Energy, 298, 117247. https://doi.org/10.1016/j.apenergy.2021.117247

[66] Sze, S. M. 2012. Physics of Semiconductor Devices: Basic Principles. McGraw-Hill: New York, NY, USA.

[67] Sze, S. M., & Ng, K. K. 2006. Photodetectors and Solar Cells. In Physics of Semiconductor Devices pp. 663–742. John Wiley & Sons, Inc.: Hoboken, NJ, USA.

[68] Vinod, R., Kumar, R., & Singh, S. K. 2018. Modeling and Simulation of Solar PV Systems: A Renewable Energy Solution. Energy Reports, 4, 701–712. https://doi.org/10.1016/j.egyr.2018.09.008

[69] Wang, F., Xuan, Z., Chen, Z., et al. 2020. Accurate solar radiation forecasting method based on real-time solar radiation mapping model. Energy Conversion and Management, 220, 113075. https://doi.org/10.1016/j.enconman.2020.113075

[70] Wang, H., Wang, B., & Su, B. 2017.

[71] World Bank. 2008. Development and Climate Change. https://doi.org/10.1596/28200

[72] X. Yuan, W. Merk, H. Stemmler, and J. Allmeling, "Stationary-frame generalized integrators for current control of active power filters with zero steady-state error for current harmonics of concern under unbalanced and distorted operating conditions," IEEE transactions on industry applications, vol. 38, no. 2, pp. 523-532, 2002.

[73] Xiao, C., Xu, E., Yang, D., & Qiu, D. 2018. Effect of Solar Irradiance and Temperature on the Performance of Compensated Crystalline Silicon Solar Cells.
Publication details to be completed—please verify the journal or source

[74] Y. Li, S. Jiang, J. G. Cintron-Rivera, and F. Z. Peng, "Modeling and control of quasi- Z-source inverter for distributed generation applications," IEEE Transactions on Industrial Electronics, vol. 60, no. 4, pp. 1532-1541, 2012.

[75] Z. Liu, J. Liu, and Y. Zhao, "A unified control strategy for three-phase inverter in distributed generation," IEEE Transactions on power electronics, vol. 29, no. 3, pp. 1176- 1191, 2013.

[76] Zhang, C., Honsberg, C., Faleev, N., & Goodnick, S. 2014. Simulation and Fabrication of High-Efficiency GaAs-Based Solar Cells. Arizona State University: Phoenix, AZ, USA.

[77] Zougo, O. 2011. Experimental and computational study of thermal and electrical performance of building-integrated photovoltaic concept in a new building. Department of Mechanical Engineering

[78] A. Thakfan and Y. Bin Salamah, "Development and Performance Evaluation of a Hybrid AI-Based Method for Defects Detection in Photovoltaic Systems," Energies, vol. 18, no. 4, p. 812, 2025.

[79] H. R. Parsa and M. Sarvi, "Online fault diagnosis, classification, and localization in photovoltaic systems," IEEE Transactions on Instrumentation and Measurement, vol. 73, pp. 1-8, 2024.

[80] A. Bebboukha, L. Chouaib, R. Meneceur, and I. Harbi, "Experimental evaluation of dead time performance in single-phase inverter MOSFETs and IGBTs under varying loads," in 2023 International Conference on Decision Aid Sciences and Applications (DASA), 2023: IEEE, pp. 635-640.

[81] A.-M. Badea, D. Manaila-Maximean, L. Fara, and D. Craciunescu, "Maximizing solar photovoltaic energy efficiency: MPPT techniques

investigation based on shading effects," Solar Energy, vol. 285, p. 113082, 2025.

[82] Y. M. Ali, L. Ding, and S. Qin, "An efficient approach for diagnosing faults in photovoltaic array using 1D-CNN and feature selection Techniques," International Journal of Electrical Power & Energy Systems, vol. 166, p. 110526, 2025.

[83] A. Bebboukha et al., "A reduced vector model predictive controller for a three-level neutral point clamped inverter with common-mode voltage suppression," Scientific Reports, vol. 14, no. 1, p. 15180, 2024.

[84] A. Demirci, I. Dagal, S. M. Tercan, H. Gundogdu, M. Terkes, and U. Cali, "Enhanced ANN-Based MPPT for Photovoltaic Systems: Integrating Metaheuristic and Analytical Algorithms for Optimal Performance Under Partial Shading," IEEE Access, 2025.

[85] K. Veni, N. S. Kumar, and J. Gnanavadivel, "Non-invasive health status diagnosis of solar PV panel using ensemble classifier," ELECTRICAL ENGINEERING, 2024.

[86] S. A. Zaki, H. Zhu, M. A. Fakih, A. R. Sayed, and J. Yao, "Deep-learning–based method for faults classification of PV system," IET Renewable Power Generation, vol. 15, no. 1, pp. 193-205, 2021.

[87] M. H. Ali, M. Zakaria, and S. El-Tawab, "A comprehensive study of recent maximum power point tracking techniques for photovoltaic systems," Scientific Reports, vol. 15, no. 1, p. 14269, 2025.

[88] A. M. Belgacem, M. Hadef, K. Kahili, M. Alshareef, M. Ghatasheh, A. Flah, and A. Hoballah, "Advanced Fault Diagnosis in Photovoltaic Arrays using a Metropolis-Hastings Convolutional Variational Autoencoder," IEEE Access, 2025.

[89] M. J. Abbass, R. Lis, and Z. Mushtaq, "Artificial neural network (ANN)-based voltage stability prediction of test microgrid grid," IEEE Access, vol. 11, pp. 58994-59001, 2023.

[90] C. Labiod et al., "Enhanced photovoltaic panel diagnostics through AI integration with experimental DC to DC Buck Boost converter implementation," Scientific Reports, vol. 15, no. 1, p. 295, 2025.

[91] W. G. Shin, H. G. Oh, S. H. Bae, Y. C. Ju, H. M. Hwang, and S. W. Ko, "Fault Diagnosis of PV String Using Deep-Learning and IV Curves," Current Photovoltaic Research, vol. 10, no. 3, pp. 77-83, 2022.

[92] S. Djaballah, A. Hechifa, M. h. Beriache, C. Beldjaatit, and K. Meftah, "Optimizing spot welding monitoring using sample entropy and advanced AI methods," Welding International, pp. 1-16, 2025.

[93] C. Saiprakash, S. R. K. Joga, A. Mohapatra, and B. Nayak, "Improved fault detection and classification in PV arrays using stockwell transform and data mining techniques," Results in Engineering, vol. 23, p. 102808, 2024.

[94] S. Russell and P. Norvig, Artificial Intelligence: A Modern Approach, 4th ed., Pearson, 2021.

[95] T. M. Mitchell, Machine Learning, McGraw-Hill, 1997.

[96] C. M. Bishop, Pattern Recognition and Machine Learning, Springer, 2006.

[97] T. Hastie, R. Tibshirani, and J. Friedman, The Elements of Statistical Learning, Springer, 2009.

[98] I. Goodfellow, Y. Bengio, and A. Courville, Deep Learning, MIT Press, 2016.

[99] Alpaydin, E., Introduction to Machine Learning, MIT Press, 2020.

[100] Shalev-Shwartz, S., & Ben-David, S., Understanding Machine Learning: From Theory to Algorithms, Cambridge University Press, 2014.

[101] Boyd, S., & Vandenberghe, L., Convex Optimization, Cambridge University Press, 2004.

[102] Guyon, I., & Elisseeff, A., “An Introduction to Variable and Feature Selection,” Journal of Machine Learning Research, 2003.

[103] Abu-Mostafa, Y. S., Magdon-Ismail, M., & Lin, H. T., Learning from Data, AMLBook, 2012.

[104] Jain, A. K., Mao, J., & Mohiuddin, K. M., “Artificial Neural Networks: A Tutorial,” IEEE Computer, 1996.

[105] Turban, E., Sharda, R., Delen, D., & King, D., Business Intelligence and Analytics: Systems for Decision Support, 10th Edition, Pearson, 2018.

[106] Russell, S., & Norvig, P., Artificial Intelligence: A Modern Approach, 4th Edition, Pearson, 2020.

[107] Liao, S. H., “Expert system methodologies and applications—a decade review from 1995 to 2004,” Expert Systems with Applications, 2005.

[108] Jiang, F., & He, Y., “AI-based fault diagnosis and predictive maintenance in electrical systems,” IEEE Transactions on Industrial Informatics, 2019.

[109] Shim, J. P., Warkentin, M., Courtney, J. F., Power, D. J., Sharda, R., & Carlsson, C., “Past, present, and future of decision support technology,” Decision Support Systems, 2002.